Smart Biotechnology

Tech Science Press

http://doi.org/10.32604/sbt.2026.092750

REVIEW

Construction of Soft Matter via Microfluidic Templates and Their Biomedical Applications

Zhonglin Fang and Chong Wang*

Institutes of Biomedical Sciences, Fudan University, Shanghai, China
*Corresponding Author: Chong Wang. Email: 20111510007@fudan.edu.cn

Received: 11 September 2026; Accepted: 09 October 2026; Published: 27 October 2026

ABSTRACT: Soft matter materials with tailored structures and functions have attracted increasing attention for applications in various fields. However, creating soft materials with complex architectures, controlled compositions, and organized spatial arrangements remains challenging. Microfluidic templating provides a powerful strategy for addressing these challenges by using well-controlled fluid flows and interfaces to guide material formation. Microfluidically-generated droplet- and jet-based templates enable the fabrication of soft matter microparticles and microfibers with tunable structures and properties. In this review, we summarize recent progress in the microfluidic fabrication of soft matter based on droplets and jets, focusing on their formation mechanisms, structural control, and integration with other fabrication methods. We further highlight the functional advantages of these engineered structures in various applications and discuss the remaining challenges and future perspectives for developing advanced soft materials through microfluidic templating.

KEYWORDS: Microfluidics; soft matter; microparticles; microfibers

1 Introduction

Soft matter represents a diverse class of materials composed of molecular or colloidal building blocks that organize into structures at the mesoscopic length scale [1–3]. Unlike conventional hard materials, which are dominated by strong covalent or metallic bonds, soft matter is governed by relatively weak and reversible interactions, such as electrostatic interactions, hydrogen bonding, hydrophobic association, and van der Waals interactions [4,5]. The delicate balance between these interactions and thermal fluctuations gives rise to dynamic and adaptive behaviors, such as self-assembly, phase separation, viscoelasticity, and structural reconfiguration [6–9]. These intrinsic characteristics enable soft matter to exhibit highly tunable structures and functions, providing unique opportunities for the development of responsive and multifunctional materials. To fully exploit these capabilities, precise control over their morphology, composition, and spatial organization is essential.

Conventional fabrication strategies, including bulk processing, lithography, and self-assembly, have enabled the construction of diverse soft materials with well-controlled architectures [10–17]. Despite these advances, the simultaneous regulation of microscale structures, internal organization, and multicomponent integration remains challenging, particularly in the fabrication of complex and hierarchical materials. Addressing these limitations requires fabrication strategies capable of precisely manipulating materials, interfaces, and their spatial organization across multiple length scales [18,19]. Among emerging fabrication strategies, microfluidic technology has attracted increasing attention owing to its ability to precisely

Copyright © 2026 The Authors. Published by Tech Science Press. This work is licensed under a Creative Commons Attribution 4.0 International License, which permits unrestricted use, distribution, and reproduction in any medium, provided the original work is properly cited.

manipulate fluids and interfaces at the microscale. This capability arises from the dominance of viscous forces over inertial forces within microchannels, where fluids typically flow in a laminar regime, allowing multiple streams to be precisely positioned with minimal convective mixing [20,21]. By controlling flow conditions, channel geometries, and fluid compositions, microfluidic systems can generate a wide range of confined structures, including droplets and jets, whose dimensions, morphologies, and compositions can be precisely regulated [22,23]. These fluidic templates can be converted into stable soft materials through solidification or interfacial processing. Combining different templates or fluid streams further allows the construction of hybrid and compartmentalized structures, enabling hierarchical architectures and multifunctional designs [24,25].

In this review, we focus on soft matter fabricated using microfluidic droplets and jets as templates and their biomedical applications (Fig. 1). We first introduce the fundamental principles of droplet- and jet-based templating and classify the resulting structures according to their characteristic fluidic configurations. Hybrid approaches that integrate droplet and jet formation are also discussed to highlight the broader structural possibilities offered by microfluidic templating. We then examine the diverse applications of these microfluidically fabricated soft materials, with particular emphasis on how their structural features translate into specific functions. Finally, we examine the remaining challenges in microfluidic templating and discuss emerging opportunities for the design and fabrication of next-generation soft matter with increasingly sophisticated structures and functions. Through this review, we aim to elucidate the relationships among fluidic templates, material architectures, and resulting functions, and to provide insights into how microfluidic templating can be further exploited for the rational design of structurally and functionally sophisticated soft materials.

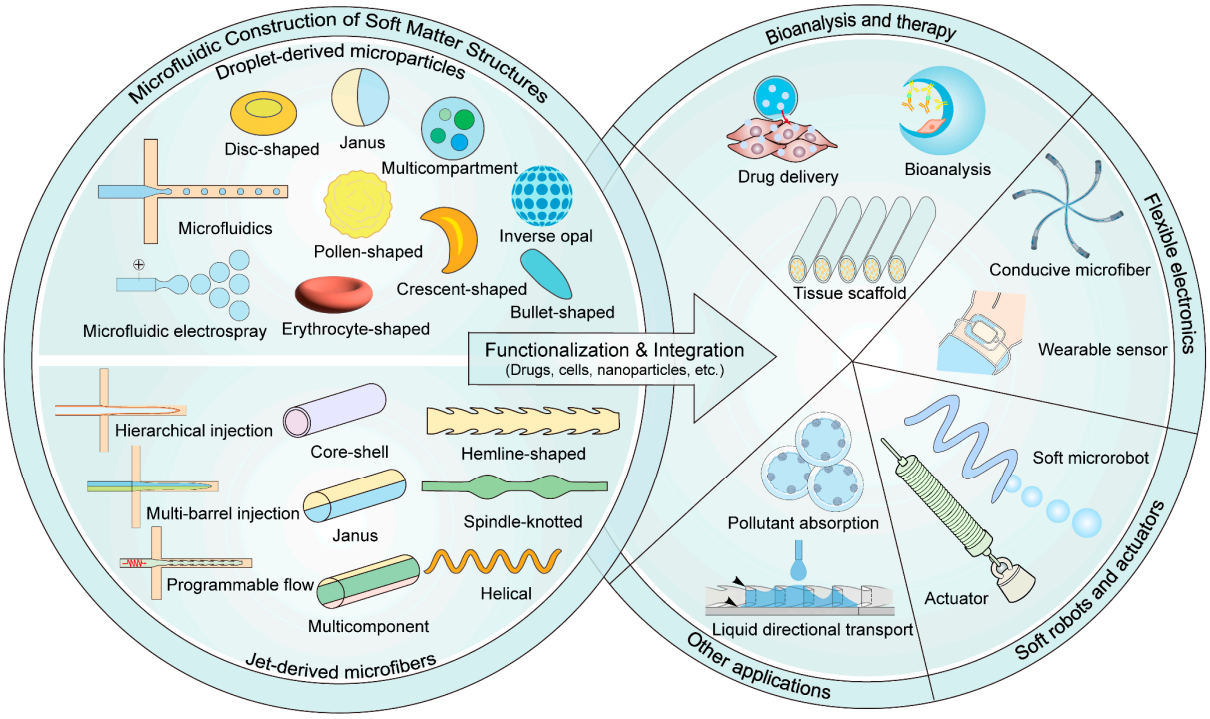


Figure 1: Schematic of droplet-derived microparticles and jet-derived microfibers fabricated via microfluidic templates and their applications.

2 Fluid Dynamics of Droplets and Jets in Microfluidics

In microfluidic systems, droplet formation occurs when a dispersed liquid is introduced through a nozzle into an immiscible continuous phase and is governed by the balance among interfacial, viscous, and inertial forces [26–28]. The relative importance of these forces can be characterized using dimensionless numbers [29]. The relative contribution of viscous effects and interfacial tension can be quantified by the Capillary number (*Ca*):

$$Ca = \frac{\eta v}{\sigma}, \tag{1}$$

where η, v and σ are the fluid viscosity, characteristic velocity, and interfacial tension, respectively. Similarly, the Weber number (*We*) characterizes the relative importance of inertial effects compared with interfacial tension:

$$We = \frac{\rho v^2 l}{\sigma}, \tag{2}$$

where ρ, v, l, and σ are the fluid density, characteristic velocity, characteristic length, and interfacial tension, respectively. At low continuous-phase flow rates, corresponding to low *Ca* and *We* values, interfacial tension dominates, causing droplets to pinch off rapidly near the nozzle in the dripping regime, which is driven by absolute instability and produces highly uniform droplets. As the flow rate increases, viscous forces increasingly overcome interfacial tension, stretching the dispersed phase into a thinning jet before pinch-off occurs [30,31]. Within the jet, inertial forces become increasingly significant, as reflected by an increasing *We*, while Rayleigh-Plateau instability amplifies perturbations along the jet, causing it to fragment downstream into polydisperse droplets [32,33]. Aqueous two-phase systems (ATPS) represent a notable case within this general framework because of their intrinsically low interfacial tension (10^{-4}~10^{-1} mN/m) [34]. This characteristic results in a naturally high *Ca* even at moderate flow rates, allowing viscous forces to dominate from the outset [35,36]. Consequently, ATPS can form stable, continuous jets without spontaneous droplet breakup, in contrast to conventional systems, in which jet formation typically requires higher flow rates [32]. Specifically, viscous forces from the continuous phase pull the dispersed fluid downstream, while interfacial tension anchors it at the nozzle and drives the pinch-off process; inertial forces become increasingly important at higher flow rates and influence jet dynamics. Consequently, droplet generation in ATPS requires external energy input, such as vibration or electric fields to disrupt the viscous-dominated jet and induce fragmentation [37–40]. Representative microfluidic strategies for generating structurally diverse microparticles and microfibers are summarized in Table 1.

Table 1: Microfluidic strategies for fabricating structurally diverse microparticles and microfibers.

Categories	Strategies	Materials	Morphology	Ref.
Microparticles	Microchannel confinement	PEGDA	Rod, disc, bullet	[41]
	Pulsed light solidification of jets	PEGDA	Bullet	[42]
	Phase separation	PEGDA, dextran	Crescent	[43]
	Gas removal	PNIPAM	Crescent	[44]
	Selective curing	Acrylamide, Al_2O_3 NPs	Crescent	[45]
	Ternary emulsion curing, template etching	Acrylate	Erythrocyte	[46]
	Osmotic pressure regulation	ALG, glycerol	Erythrocyte	[47]
	Colloidal self-assembly, solvent extraction	Silica NPs, hydrogels	Suction-cup	[48]

Table 1: *Cont.*

Categories	Strategies	Materials	Morphology	Ref.
Microparticles	Droplet freezing	PEGDA, dextran	Cradle	[49]
	Solvent evaporation	PLGA-b-PEG/PLGA	Pollen	[50]
	Regional polymerization	ALG, $CaCl_2$ aerosol	Crater-terrain	[51]
	Confined self-assembly, template etching	HAMA, SFMA	Inverse opals	[52]
	Droplet dripping	ALG	Teardrop, jellyfish, cap, donut	[4]
	Viscosity control	ALG, PEG/dextran/glycerol	Teardrop, mushroom, peach, dimple	[53]
	Polymer blend phase separation	PS, PMMA, PLA	Janus	[54]
	Hierarchical emulsion templates	ALG, Ca-EDTA	Multicompartment	[55]
	Parallel multi-inlet flows	ALG	Multicompartment	[56]
	Alternating injection, selective degradation	ALG, GelMA	Multicompartment	[57]
	Dispersing microspheres into inner fluid	ALG, GelMA	Multicompartment	[58]
	Colloidal crystal assembly	PAM, Silica NPs	Inverse opals	[59]
	Microfluidic encapsulation	PLGA	Capsules	[60]
	Biomimetic microstructure fabrication	Chitosan, ALG, cellulose	Wrinkled	[61]
	Piezoelectric vibration	PEGDA, GO/NIPAM	Jellyfish	[62]
Microfibers	Hierarchical capillaries	ALG, HA	Hollow, core-shell, double-layered	[63]
	Microfluidic 3D printing	ALG, NIPAM, PVA	Hollow, scaffold	[64]
	Multi-barrel capillaries	RGD-ALG	Multicompartment	[65]
	Emulsification-spinning synergy	ALG, GelMA	Spindle-knotted	[65]
	Dehydration shrinkage	ALG, ETPTA	Spindle-knotted	[66]
	Piezoelectric vibration	PEGDA, ALG	Spindle-knotted	[67,68]
	Flow control	ALG	Helical	[69]
	Centrifugal assembly	Silica NPs, n-butylacrylate	Twisted	[68]
	Piezoelectric vibration	PEGDA	Hemline	[70]
	Valve-controlled sequential injection	P(NIPAM-co-AAc), ALG	Axially patterned	[71]
	Multiflow microfluidics	PEDOT:PSS, ALG	Core-shell	[72]
	Microfluidic 3D printing	ALG, PAAm	Scaffold	[73]
	Microfluidic spinning	ALG	Core-shell	[74]
	Microfluidic spinning	PVDF-HFP, GO	Porous, wrinkled	[75]
	Flow control	PEGDA, ALG	Helical	[23]

Abbreviations: AAc, acrylic acid; ALG, alginate; Ca-EDTA, calcium ethylenediaminetetraacetate; ETPTA, ethoxylated trimethylolpropane triacrylate; GelMA, methacrylated gelatin; GO, graphene oxide; HA, hyaluronic acid; HAMA, hyaluronic acid methacrylate; NIPAM, N-isopropylacrylamide; NPs, nanoparticles; PAAm and PAM, polyacrylamide; PEDOT, poly(3,4-ethylenedioxythiophene); PSS, poly(styrene sulfonate); PEG, poly(ethylene glycol); PEGDA, poly(ethylene glycol) diacrylate; PLA, poly(lactic acid); PLGA, poly(lactic-co-glycolic acid); PLGA-b-PEG, poly(lactic-co-glycolic acid)-block-poly(ethylene glycol); PMMA, poly(methyl methacrylate); PNIPAM, poly(N-isopropylacrylamide); PS, polystyrene; PVA, poly(vinyl alcohol); PVDF-HFP, poly(vinylidene fluoride-co-hexafluoropropylene); RGD-ALG, arginine-glycine-aspartic acid-functionalized alginate; SFMA, silk fibroin methacrylate.

3 Droplet-Derived Soft Matter Structures

Droplets are versatile building blocks for soft matter fabrication because of their highly tunable structures in microfluidic systems. Under equilibrium conditions, droplets tend to adopt a spherical shape due to surface tension. Spherical droplet-derived soft matter structures, such as solid microspheres and core–shell microcapsules, have been extensively reported [38,76–82]. Microfluidics can also enable the fabrication

of heterogeneous structures through precise control of channel design, component selection, and fluid flow. Therefore, this section focuses exclusively on heterogeneous droplet-derived soft matter structures.

3.1 Morphologically Heterogeneous Structures

Morphological heterogeneity refers to nonspherical or topologically complex shapes in droplet-derived soft matter. Unlike simple non-spherical particles, morphologically complex structures exhibit distinct geometric features, such as elongated tips, internal cavities, and surface wrinkles, that arise from controlled droplet deformation during microfluidic processing [41–43,45–50]. These structures are particularly valuable for mimicking natural biological morphologies and optimizing performance in applications such as vascular embolization, mucosal adhesion, and cell guidance.

3.1.1 Common Nonspherical Morphologies

Forming non-spherical structures is relatively challenging because liquids tend to adopt a spherical shape to minimize their surface energy. Nonspherical morphologies discussed in this review mainly include rod-, disc-, and bullet-shaped particles, as well as crescent- and erythrocyte-shaped particles. These morphologies are mainly generated by deforming droplets via microchannel confinement, fluid impact, or interfacial instability, followed by rapid solidification to preserve the deformed state. Microfluidics enables precise tuning of these morphologies by adjusting hydrodynamic parameters and channel geometry.

Rod-, disc-, and bullet-shaped particles In the microfluidic synthesis of rod-, disc-, and bullet-shaped particles, a common underlying principle is the spatial confinement imposed by microchannels, which regulates particle morphology by restricting the spatial expansion of precursors [83,84]. However, their distinct morphologies arise from differences in channel design and the interplay between geometric confinement and growth kinetics [85,86]. For rod-like particles, elongated cylindrical or rectangular microchannels with a high length-to-width ratio are typically used (Fig. 2A) [41]. The axial direction provides sufficient space for precursor elongation, whereas radial growth is restricted by the narrow channel cross section, resulting in anisotropic growth and an increased axial dimension. In addition to crosslinking rod-shaped droplets, another approach for producing such particles is the use of pulsed light to solidify jets into discrete particles (Fig. 2B) [42]. For disc-like particles, flat rectangular channels with a small height-to-width ratio are preferred. The in-plane direction allows lateral growth, whereas the out-of-plane direction is tightly confined, resulting in flattened, disc-shaped structures with a large aspect ratio in the planar dimensions (Fig. 2A). In contrast, bullet-like particles are typically formed in gradient microchannels, where the progressively changing channel geometry generates a nonuniform flow field and asymmetric hydrodynamic stresses around the precursor droplets (Fig. 2C) [87]. The combined effects of geometric confinement and flow-induced deformation produce the characteristic bullet-like morphology with a pointed front and a blunt rear.

Crescent- and erythrocyte-shaped particles Concave particles represent another class of morphologically heterogeneous structures and can be classified into single-sided and biconcave shapes, commonly referred to as crescent-shaped and erythrocyte-shaped particles, respectively. Crescent-shaped particles can be prepared by solidifying one phase while removing the other, thereby creating a single-sided depression [44,88–90]. A classic approach involves phase separation. For example, droplets containing two water-soluble polymers, PEGDA and dextran, undergo phase separation due to their thermodynamic incompatibility, forming droplets with an asymmetric distribution of a solidifiable phase and a sacrificial phase. Upon ultraviolet (UV) curing of the PEGDA phase, the sacrificial dextran phase was washed away, leaving a PEGDA particle with a single-sided depression (Fig. 2D) [43]. Similarly, gas-liquid Janus droplets formed via

microfluidics can generate concave structures after the gas phase is removed following curing [44]. In addition, Li's team exploited the UV absorption and scattering properties of Al_2O_3 nanoparticles to selectively cure the droplet surface while leaving a depression, enabling the fabrication of ceramic crescent-shaped particles (Fig. 2E) [45].

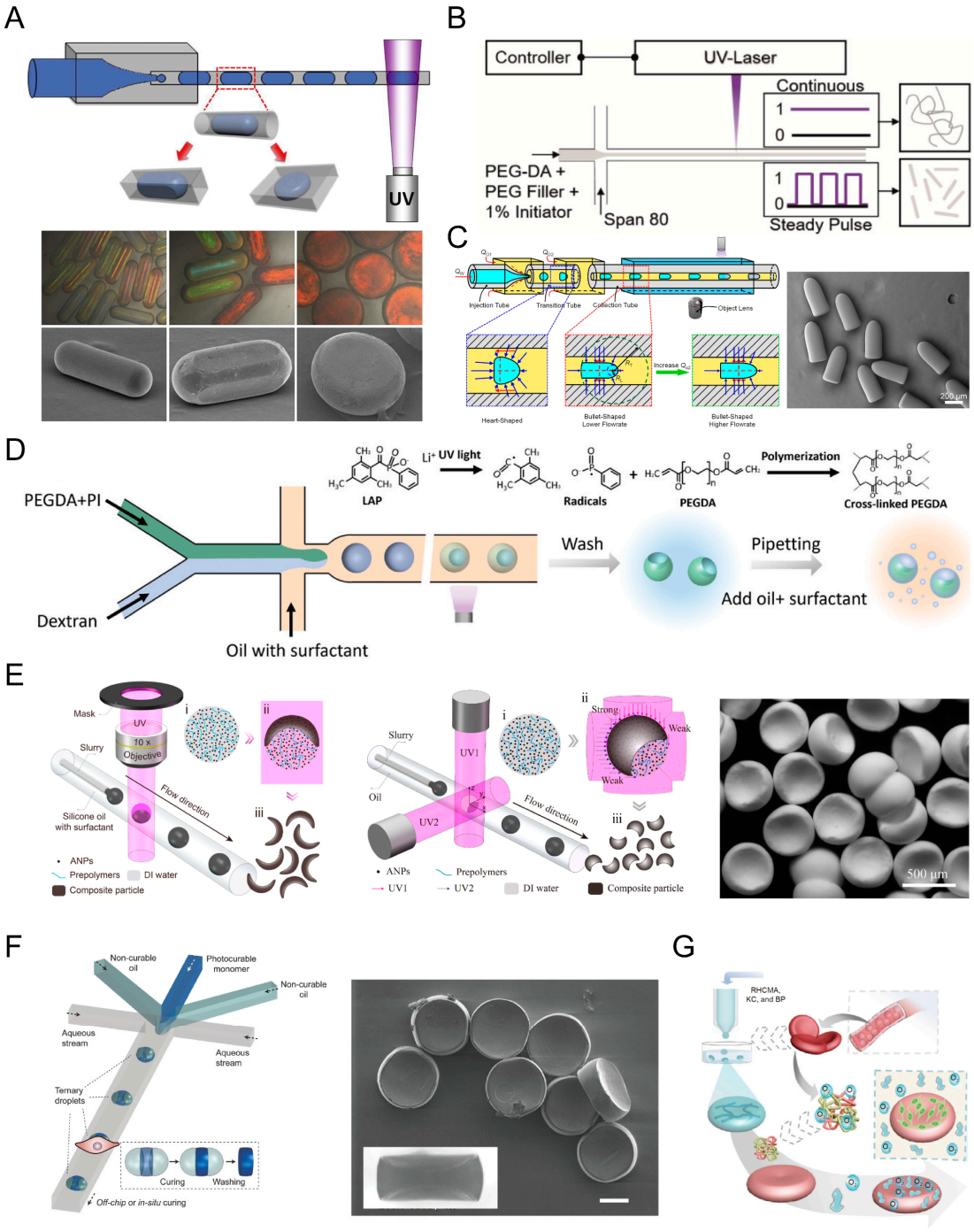


Figure 2: Microfluidic fabrication of nonspherical droplet-derived soft matter. (**A**) Rod- and disc-shaped particles prepared via confined microchannels [41]. (**B**) Bullet-shaped particles fabricated by pulsed-light solidification of jets [42]. (**C**) Bullet-shaped particles formed in gradient microchannels [87]. (**D**) Crescent-shaped particles prepared

via phase separation of PEGDA and dextran [43]. (**E**) Crescent-shaped ceramic particles fabricated by selective curing using Al_2O_3 nanoparticles. (**i**) Slurry droplets containing Al_2O_3 nanoparticles and UV-curable prepolymers; (**ii**) selective UV curing due to the attenuation of UV light by the nanoparticles; (**iii**) the resulting crescent-shaped particles [45]. (**F**) Erythrocyte-shaped particles generated from ternary emulsion droplets. Scale bar: 50 μm [46]. (**G**) Erythrocyte-shaped particles fabricated via microfluidic electrospray with glycerol-regulated osmotic pressure [47].

To prepare erythrocyte-shaped particles, depressions are introduced on both sides of the droplet. Erythrocyte-shaped particles can be prepared using microfluidics to generate ternary emulsion droplets with a "solidified phase-double non-solidified phase" configuration via microfluidics. Capillary forces confine the non-solidified phases, and subsequent photopolymerization followed by removal of the uncured phases produces a symmetric erythrocyte-shaped structure (Fig. 2F) [46]. Another approach relies on regulating the hydrodynamic flow field within microfluidic channels. By tuning the flow-field intensity, symmetric stagnation zones can be generated at both ends of the droplets. Hydrodynamic forces drive the material toward the droplet periphery, leaving a thin central layer and inducing depressions on both sides, thereby forming erythrocyte-shaped particles through phase separation and solidification [91]. In microfluidic electrospray, glycerol can be added to the collection liquid to regulate osmotic pressure. When the droplets are crosslinked in the collection dish, the resulting osmotic pressure gradient causes them to preferentially shrink from both sides, producing the characteristic erythrocyte shape (Fig. 2G) [47].

3.1.2 Topologically Complex Morphologies

Microfluidic technologies also enable precise control over the fabrication of soft matter microparticles with complex topologies, allowing the customization of diverse structural features. One class of such microparticles features semi-open architectures that can be created through phase transitions or colloidal self-assembly within microfluidic droplets. For suction-cup-like microparticles, monodisperse silica nanoparticles are dispersed in an aqueous phase and emulsified into droplets using microfluidics (Fig. 3A) [48]. Rapid solvent extraction induces asymmetric self-assembly of the nanoparticles, causing the top of the droplet to fold inward and form a concave structure. This colloidal crystal template can be replicated using hydrogels while preserving the suction-cup-like morphology. Another semi-open design, cradle-shaped microgels, can be fabricated by generating water-in-oil (W/O) droplets [49]. Cooling the oil phase below its freezing point causes volume shrinkage and collapse of the aqueous droplet core, forming a concave cavity that is subsequently stabilized by UV crosslinking of the prepolymers.

Microfluidics also enables the fabrication of microparticles with specific surface topologies. Pollen-inspired microparticles with rough surfaces can be fabricated using microfluidic oil-in-water (O/W) droplets containing polymer blends dissolved in a volatile solvent [50]. As the solvent evaporates, interfacial instabilities induce the formation of surface wrinkles or protrusions, whose density and morphology can be tuned by adjusting the polymer blend ratio (Fig. 3B). Similarly, crater-terrain hydrogel microparticles can be fabricated by combining droplet-aerosol impact with localized polymerization [51]. Alginate (ALG) droplets pass through a $CaCl_2$ aerosol zone, where aerosol impact generates transient surface cavities. Subsequent localized crosslinking stabilizes these cavities, resulting in a lunar crater-like surface with tunable crater density that can be adjusted by varying the aerosol parameters (Fig. 3C).

Another category of topologically defined microparticles is inverse opal microparticles, which feature periodic, interconnected porous frameworks [52]. These structures are fabricated through microfluidic-induced confined self-assembly of silica nanoparticles into spherical colloidal crystals. The resulting crystals are then infiltrated with a UV-polymerizable hydrogel precursor. After UV curing, the silica template is

etched away using hydrofluoric acid, leaving an inverse opal structure with ordered pores that retain the periodicity of the original colloidal crystal (Fig. 3D).

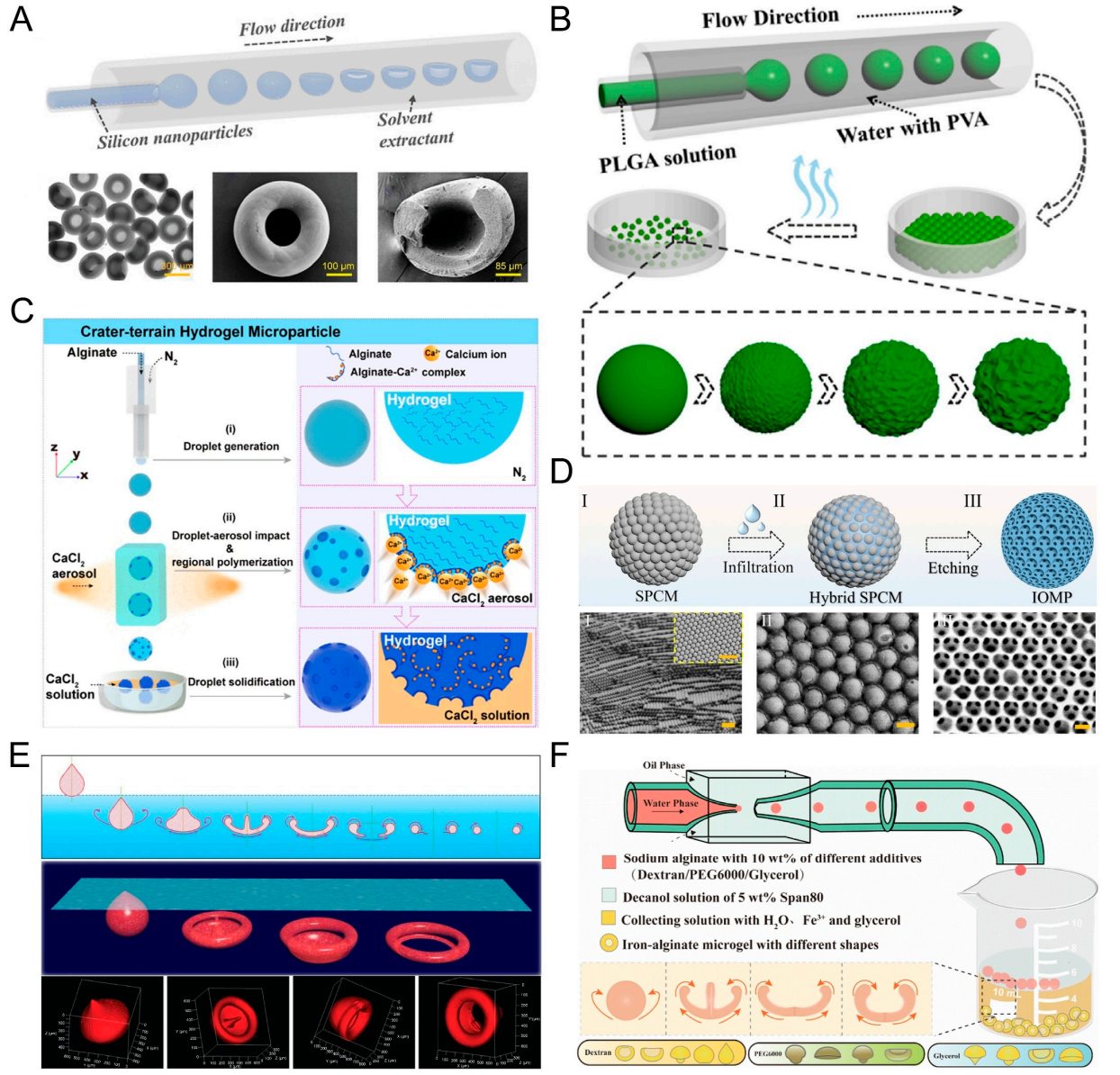


Figure 3: Microfluidic preparation of topologically complex microparticles. (**A**) Suction-cup-like microparticles fabricated via colloidal self-assembly and solvent extraction [48]. (**B**) Pollen-inspired microparticles with rough surfaces fabricated from polymer-blend O/W droplets [50]. (**C**) Crater-terrain hydrogel microparticles fabricated by droplet-aerosol impact and localized polymerization [51]. (**D**) Inverse opal microparticles fabricated via confined self-assembly of silica nanoparticles. Scale bars: 1 μm [52]. (**E**) Unconventional microparticles induced by droplet impact and viscosity control [4]. (**F**) Various microgel morphologies tuned by additives in ALG droplets [53].

During microparticle formation, variations in droplet impact, viscosity, and crosslinking can drive distinct deformation behaviors, producing diverse unconventional shapes. For example, droplet impact on a miscible liquid surface induces deformation, forming vortex rings. Droplets transition through teardrop, jellyfish, cap-like, and eventually ring-like shapes before undergoing gelation or precipitation, resulting

in four distinct particle shapes (Fig. 3E) [4]. Droplet viscosity and impact speed govern the evolution of the vortex rings and the resulting particle morphology. Higher viscosity slows diffusion and favors the formation of cap-like shapes, whereas higher impact speeds accelerate curling and promote the formation of ring-like structures. Adjusting the collection height also affects droplet deformation, with lower collection heights leading to tail-like shapes and higher heights producing dented shapes. In addition, glycerol in the gel bath can adjust the viscosity, thereby regulating ion diffusion and promoting the formation of specific morphologies, such as mushroom-like shapes. Through the combined effects of these factors, microparticles with mushroom-, hemispherical, erythrocyte-, pear-, tail-, and dented morphologies can be produced. Chen et al. used ALG solutions containing additives, including dextran, PEG, and glycerol, to generate monodisperse droplets via microfluidics [53]. These additives modify droplet viscosity, enabling precise control over particle morphology. The droplets were subsequently collected in a solution containing glycerol and Fe^{3+} crosslinking agents, which induced specific deformations and resulted in various microgel morphologies, including teardrop-, peach-, cap-, mushroom-, erythrocyte-, and sharp-tailed mushroom-like shapes (Fig. 3F).

3.2 Compositionally Heterogeneous Structures

Component heterogeneity in droplet-derived soft matter refers to the spatial segregation of distinct chemical or functional components within a single structure, enabling the integration of multiple properties without mutual interference. Microfluidics could achieve this by precisely manipulating multiphase fluid flows to generate droplets with asymmetric phase distributions. Two representative classes of such complex structures are highlighted below.

3.2.1 Janus Microparticles

Janus microparticles feature two chemically or physically distinct domains within a single structure. Their asymmetric design is particularly useful for applications requiring orthogonal functions, such as targeted delivery and dual-modal sensing, because each domain can be independently functionalized [92,93]. A typical approach for fabricating microfluidic Janus particles involves generating biphasic droplets followed by rapid curing to stabilize the anisotropic structure, often using a θ-shaped microchannel device (Fig. 4A) [94]. Another approach relies on phase separation, exploiting the thermodynamic incompatibility of polymer blends confined within microfluidically generated emulsion droplets. As the solvent evaporates, spontaneous phase separation of the polymers occurs, resulting in the formation of Janus structures (Fig. 4B) [54]. This method is similar to the fabrication of crescent-shaped microparticles, but differs in that both phases of the Janus particles are solidified, whereas crescent-shaped particles require the removal of the non-solidifiable phase. In addition, droplet-templated phase separation combined with nanoparticle self-assembly enables the formation of two domains with distinct properties within droplets composed of a single material. For example, Wang et al. used a mixture of silica nanoparticles and graphene oxide (GO) dispersed in a silicone oil continuous phase [59]. Phase separation and stratification were achieved through the density difference between GO and silica nanoparticles, together with colloidal instability induced by variations in pH. Similarly, Shang et al. encapsulated silica and Fe_3O_4 magnetic nanoparticles within droplets [95]. Under an external magnetic field, sedimentation of the magnetic nanoparticles, combined with differences in colloidal stability, accelerated the phase separation process.

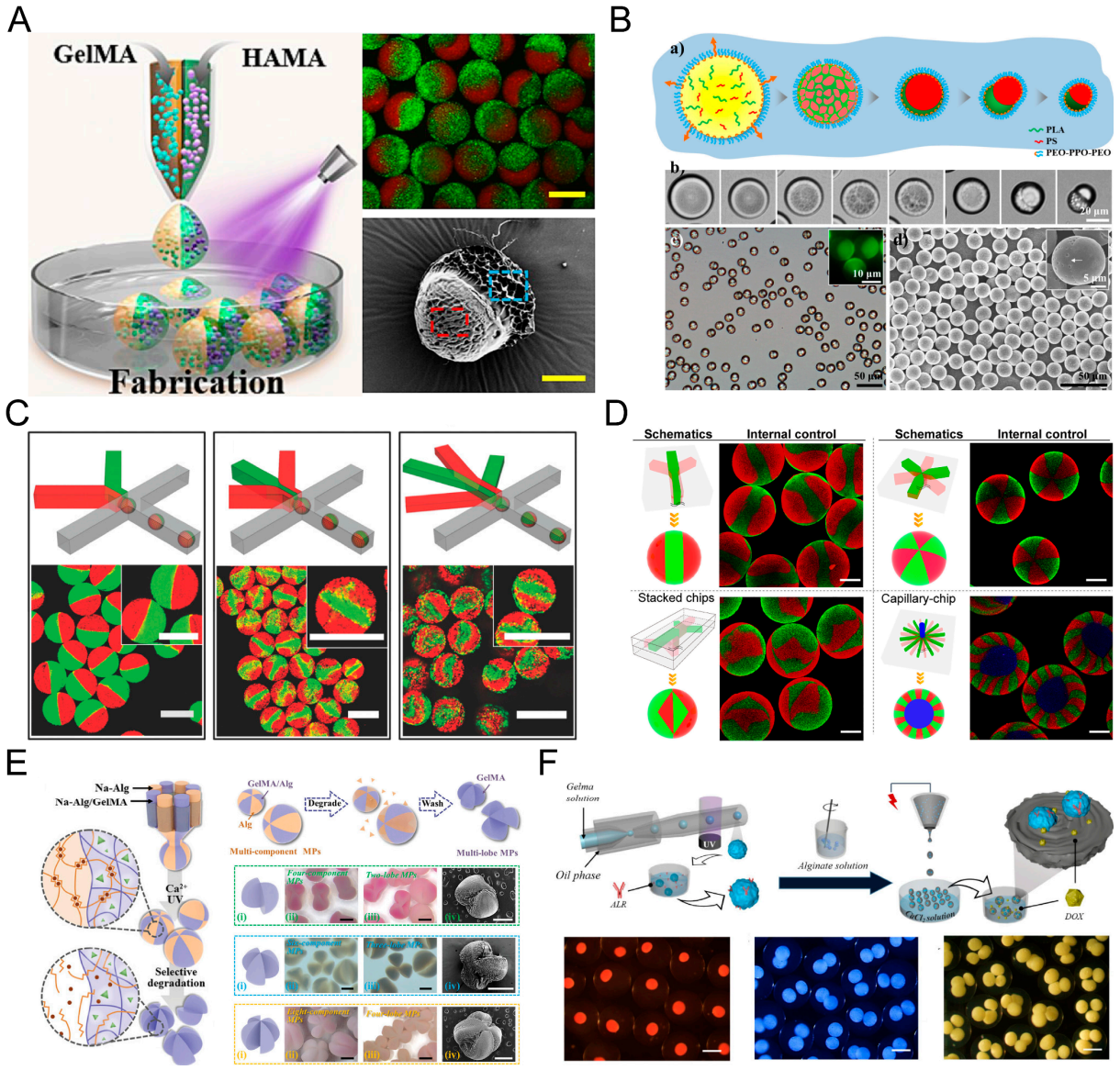


Figure 4: Microfluidic fabrication of compositionally heterogeneous droplet-derived microparticles. (**A**) Janus microparticles fabricated via biphasic droplets in θ-shaped microchannels. Scale bars: 500 μm (upper image) and 100 μm (lower image) [94]. (**B**) Janus microparticles fabricated by polymer phase separation within emulsion droplets [54]. (**C**) Multicompartment cell-laden microparticles fabricated using different numbers of inner fluid channels. Scale bars: 100 μm [55]. (**D**) Multicompartment microparticles fabricated via parallel internal fluid channels. Scale bars: 200 μm [56]. (**E**) Multi-lobed multicompartment microspheres fabricated by selective degradation of ALG components. Scale bars: 300 μm [57]. (**F**) Multicompartment particles fabricated by dispersing small microspheres in a second inner fluid. Scale bars: 200 μm [58].

3.2.2 Multicompartment Microparticles

Multicompartment microparticles represent a more complex form of component heterogeneity, featuring three or more isolated compartments within a single structure. Each compartment can function as an independent microreactor or cargo carrier, enabling the spatiotemporal regulation of different cargoes and mimicking hierarchical biological structures [96]. Microfluidic fabrication of multicompartment microparti-

cles typically relies on hierarchical emulsion templates or parallel multi-inlet flows to generate droplets with segregated internal phases [97–99]. A notable example from the David A. Weitz group involves the fabrication of bi-, tri-, and quadripartite cell-laden microparticles using different numbers of inner fluid channels, with the bipartite particles representing Janus structures (Fig. 4C) [55]. Despite the use of the same prepolymer solution in each channel, compartment formation remains unaffected. The laminar flow regime characteristic of microfluidic systems enables precise spatial confinement of the precursor phases, while subsequent rapid curing kinetically preserves the resulting compartmental architecture. This combination allows even fluids with the same matrix composition to form defined multicompartment microgels. Similarly, Lin and colleagues integrated multiple parallel internal fluid channels into a microfluidic chip, with the number of channels corresponding to the desired number of compartments [56]. These channels converge into a single merging chamber, where the multiphase flows are guided in parallel under laminar flow conditions. This setup enables the creation of up to 21 compartments (Fig. 4D). Compartmentalization can be further modified by selectively degrading one component of the multicompartment structure, as demonstrated in the formation of multi-lobed structures. For example, alternating injections of pure ALG solution and an ALG–methacrylated gelatin (GelMA) mixture into eight-barrel capillaries produce microgels with eight alternating compartments [57]. Selective degradation of the pure ALG compartments using sodium citrate results in 2-, 3-, and 4-lobed multicompartment microspheres (Fig. 4E). Another simpler approach to creating multicompartment particles involves first preparing small microspheres and then incorporating them as dispersed components into a second fluid, where shear forces induce their partitioning and the formation of multicompartment structures (Fig. 4F) [58]. The number of compartments can be tuned by varying the proportion of small microspheres to the second inner fluid.

4 Jet-Derived Soft Matter Structures

Microfluidically generated jets provide versatile templates for the fabrication of soft matter microfibers. Depending on whether the jet remains uniform or undergoes structural variation along its axial direction, the resulting fibers can exhibit either homogeneous or spatially differentiated structures. Accordingly, jet-derived microfibers can be broadly classified into two categories: those templated from axially uniform jets and those derived from axially varying jets. The following discussion focuses on the underlying fabrication mechanisms and structural characteristics of these two classes of microfibers.

4.1 Microfibers with Axially Uniform Jets as Templates

Axially uniform jets maintain a consistent overall structure along the flow direction without periodic or programmed axial variation. Here, axial uniformity refers to the preservation of this structural pattern along the fiber length rather than to chemical homogeneity. The structural diversity of microfibers formed by axially uniform jets is determined by the design of the injection capillaries in microfluidic systems. Capillaries with tapered, hierarchical, or multi-barrel configurations manipulate laminar flow patterns, directly influencing the resulting fiber architecture [100–103]. The foundational microfiber types such as solid, hollow, and hollow double-layered were systematically described by Wei et al. (Fig. 5A) [63]. Solid microfibers are formed from a single ALG stream, yielding uniform, nonporous cross sections. Hollow microfibers incorporate a hyaluronic acid fugitive core that dissolves after fabrication, leaving a central lumen. Similar to hollow microfibers, core–shell microfibers are fabricated using hierarchical injection capillaries, with the key difference being whether the material in the inner phase is crosslinked or subsequently dissolved [65]. Hollow double-layered microfibers are created from four coaxial fluid streams, with the flow rates tuned to control layer thickness and maintain axial uniformity. These basic structures

serve as templates for more complex designs, providing a foundation for further structural optimization. Another advancement in microfiber fabrication is the integration of microfluidic capillary devices with 3D printing, as reported by Wang et al. (Fig. 5B) [64]. This approach uses multi-injection glass capillaries as 3D printer nozzles, enabling the layer-by-layer stacking of hollow microfibers to construct macroscale scaffolds. The design retains the core fugitive fluid (PVA) and outer phase, consisting of black phosphorus, Na-ALG, and N-isopropylacrylamide, to form hollow fibers with 1–3 channels. The 3D printing process preserves the uniform channel structure of individual fibers while enabling precise control over their spatial arrangement, thereby bridging microscale structural uniformity with macroscale architectural control.

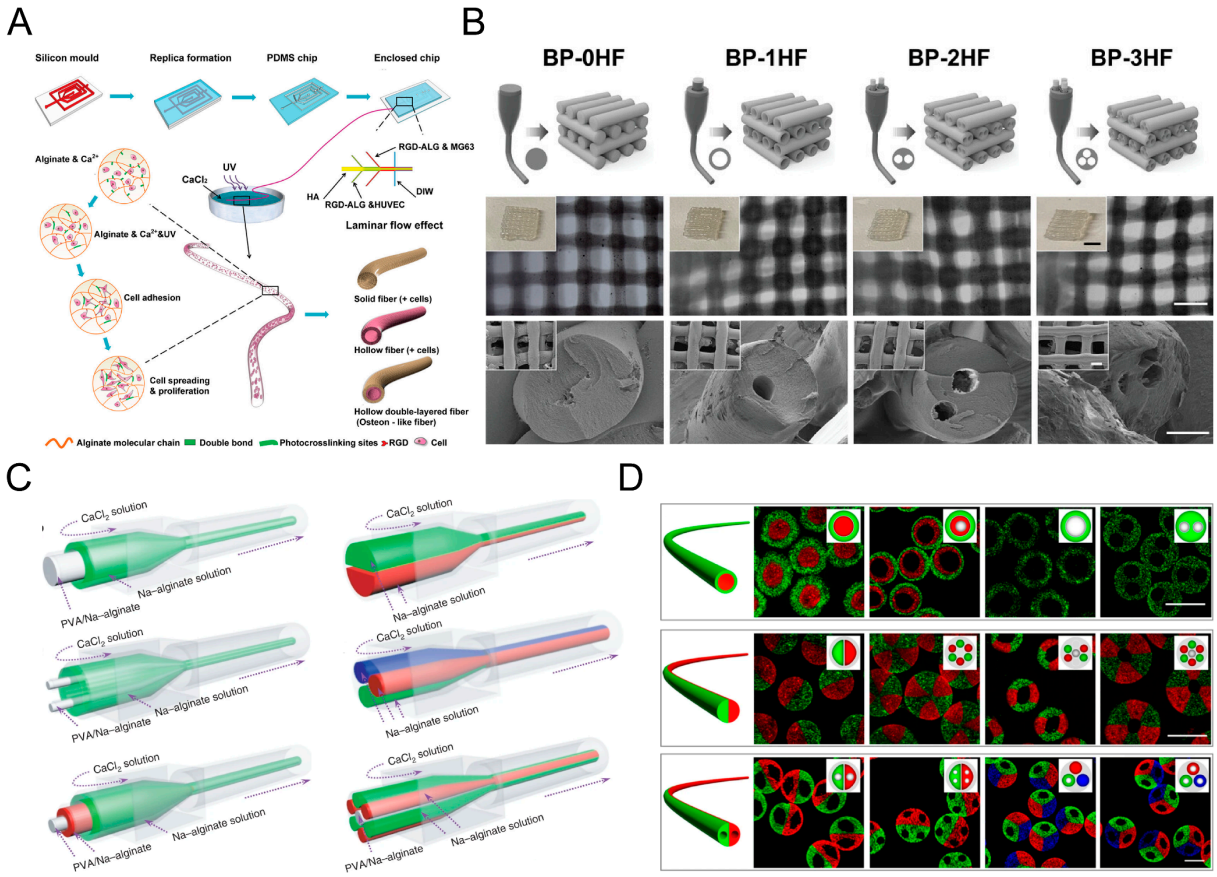


Figure 5: Axially uniform jet-templated microfibers fabricated via microfluidics. (**A**) Basic microfiber structures fabricated using tapered and hierarchical capillaries [63]. (**B**) 3D-printed macroscale scaffolds composed of hollow microfibers using integrated microfluidic capillaries. Scale bars: 1 mm (upper images) and 100 μm (lower images); 5 mm (upper inset images) and 200 μm (lower inset images) [64]. (**C**) Channel designs of different capillary configurations [65]. (**D**) Multicompartment microfibers fabricated using multi-barrel capillaries. Scale bars: 200 μm.

Multi-barrel injection capillaries, including two-barrel (θ-type), three-barrel, and seven-barrel designs, enable the fabrication of multicompartment microfibers through parallel laminar flows (Fig. 5C,D) [65]. In a θ-type capillary, two side-by-side barrels deliver distinct Na-ALG solutions, while the low Reynolds number suppresses interfacial mixing and diffusion between the streams. Simultaneous gelation with $CaCl_2$ stabilizes the Janus structure, preserving a sharp intercompartment boundary and ensuring axial uniformity. Scaling up to three- or seven-barrel capillaries extends this principle to three- or six-compartment fibers, respectively, with each barrel independently delivering a distinct precursor. For example, a seven-barrel

capillary can generate hollow microfibers with six-compartment shells. Adjusting the flow rate of each barrel controls the relative volume of each compartment, thereby ensuring uniform compartment dimensions along the fiber length.

4.2 Microfibers with Axially Varying Jets as Templates

Unlike axially uniform jets, axially varying jets are characterized by periodic or programmable variations in morphology, diameter, or composition along the flow direction. These jets are typically generated by external perturbations or dynamic fluidic interactions that disrupt the stability of laminar flow while maintaining precise control [40,104,105]. For example, piezoelectric vibration is a key strategy for generating such jets. In this approach, a piezoelectric actuator is attached to the injection capillary and transmits periodic mechanical vibrations to the inner fluid, inducing synchronous oscillations of the jet interface [70]. Upon solidification, these temporal variations in the jet are translated into spatially periodic or heterogeneous features along the resulting microfiber, enabling the fabrication of fibers with programmable architectures and spatially differentiated functions. Microfibers derived from such jets exhibit anisotropic features that confer unique functionalities, including directional liquid transport, stimulus responsiveness, and programmable actuation.

4.2.1 Spindle-Knotted Microfibers

Spindle-knotted microfibers are templated from jets with periodic knots separated by uniform joints, inspired by the fog-harvesting capability of spider silk. The core design principle involves inducing controlled deformation of fluid jets or droplets, followed by rapid solidification to preserve the spindle-knotted architecture. The most widely adopted fabrication approach combines microfluidic emulsification with spinning. As demonstrated by Yu et al., this strategy integrates sequential spinning, fluid coating, and knot emulsification (Fig. 6A) [65]. The inner ALG forms a continuous fiber backbone via ionic crosslinking, while the middle GelMA pregel is emulsified into discrete droplets by an immiscible outer oil phase at the capillary tip. These droplets deform into spindle-shaped structures and become strung along the inner fiber, where they are subsequently solidified to form stable knots. A variation of this method involves encapsulating discrete droplets within the fiber matrix during spinning, followed by dehydration-induced shrinkage. Wu et al. reported that ALG–GO fibers containing encapsulated ETPTA droplets form spindle knots as the hydrogel matrix shrinks around the droplets, exploiting the difference in elasticity between the matrix and encapsulated phases [66].

Active microfluidics has emerged as a programmable alternative for spindle-knotted microfiber fabrication. By attaching a piezoelectric actuator to the inner fluid channel, periodic mechanical vibrations are transmitted to the pregel jet, inducing synchronous oscillatory deformation and generating a wavy template. Yang et al. demonstrated that the frequency and amplitude of the piezoelectric signal directly regulate the knot wavelength and height, respectively, while stepwise adjustments in frequency or amplitude enable the generation of gradient or symmetric knot configurations [67,106]. In piezoelectric systems, frequency is inversely related to knot spacing, whereas amplitude positively correlates with knot height, enabling on-demand programming of uniform, gradient, or asymmetric structures. Unlike emulsification-based methods, this approach generates knots via pulsation of a single jet, thereby maintaining compositional homogeneity along the fiber axis.

4.2.2 Helical and Twisted Microfibers

Helical and twisted microfibers, featuring chiral, stretchable, and anisotropic structural characteristics, are representative axially varying microfibers inspired by natural helical architectures such as DNA and bacterial flagella. Their fabrication and structural regulation rely on the precise manipulation of fluid dynamics, external stimuli, or post-spinning reshaping in microfluidic systems. Diverse strategies have been developed to achieve controllable helical geometries and structural versatility [69,107].

The core preparation strategies span multiple microfluidic paradigms, beginning with coaxial capillary microfluidics that exploits unbalanced fluidic friction. In this approach, the core ALG fluid and sheath $CaCl_2$ solution flow in opposite or coaxial directions. When the inner flow rate exceeds a critical threshold relative to the outer flow rate, the accumulated elastic energy in the high-viscosity inner jet triggers a coiling instability, leading to helical deformation before *in situ* solidification (Fig. 6B) [69]. This method enables the continuous fabrication of helical microfibers with highly tunable structural parameters, including single-, double-, and multicomponent helical architectures, through modifications of the injection capillary design.

Centrifugal assembly represents another key strategy, in which rotating outer capillaries generate helical flow patterns by superimposing axial flow and drag flow (Fig. 6C) [68]. The direction of the centrifugal force, determined by the density difference between the fiber precursor and the surrounding fluid, is critical for stable helical assembly. First, the low-density fiber precursor is drawn toward the channel center, minimizing contact with the channel walls and preventing destructive collisions, while subsequent changes in density facilitate controlled collection. This method enables the integration of multiple fibers into double or triple helices by adjusting the number of extrusion nozzles. Coaxial microfluidics enables the integration of distinct components into helical fibers with sharp intercompartment boundaries, whereas centrifugal assembly and reshaping strategies support the fabrication of multifiber twisted microropes and helices with tunable pitch or radius.

4.2.3 Hemline-Shaped and Programmable Microfibers

Recent advances in piezoelectric microfluidics have enabled the fabrication of hemline-shaped microfibers templated from jets with periodic corrugations featuring sharp edges and wedge-shaped corners. These jets are generated via programmed piezoelectric vibration of the inner fluid, which induces controlled jet deformation before polymerization. The resulting fibers exhibit axially varying cross sections with annularly connected microcavities, enabling directional liquid transport through asymmetric pinning and capillary rise effects (Fig. 6D) [70]. The inner phase can be designed as either a photocurable solution or a sacrificial template, depending on whether solid or hollow fibers are desired [70,108]. In a typical coaxial microfluidic configuration, the inner phase is dynamically perturbed by programmable piezoelectric signals, generating a corrugated jet template under laminar flow conditions. The outer phase can then be polymerized to solidify the transient hemline-shaped structure, while the sacrificial inner phase is subsequently removed to form the characteristic microcavity architecture [108]. The piezoelectric frequency is inversely correlated with the hemline pitch, whereas the piezoelectric amplitude regulates the hemline length.

Another approach to developing programmable microfibers involves valve-controlled microfluidic systems. Takeuchi et al. reported microfibers with functional programmability achieved through axial patterning of stimuli-responsive (SR) and non-responsive hydrogel regions [71]. Their fabrication relies on computer-programmed actuation of pneumatic valves to regulate the sequential injection of SR and non-responsive precursor solutions, enabling flexible control over the position, length, and distribution of SR regions along the fiber axis. The programmable deformation of these fibers arises from the differential swelling or shrinkage of the SR regions in response to external stimuli, inducing local bending or self-folding

into predefined three-dimensional (3D) structures. Notably, the chirality of the folded structures can be tuned by varying the mode of stimulus application: uniform stimulation induces a mixture of left- and right-handed helices, whereas sequential stimulation yields predominantly single-handed chirality, reflecting the fiber's sensitivity to the spatial and temporal pattern of perturbation. Optimizing the cross-sectional proportion of SR regions further ensures stable steady-state patterning, thereby enabling consistent and reproducible responsive behavior.

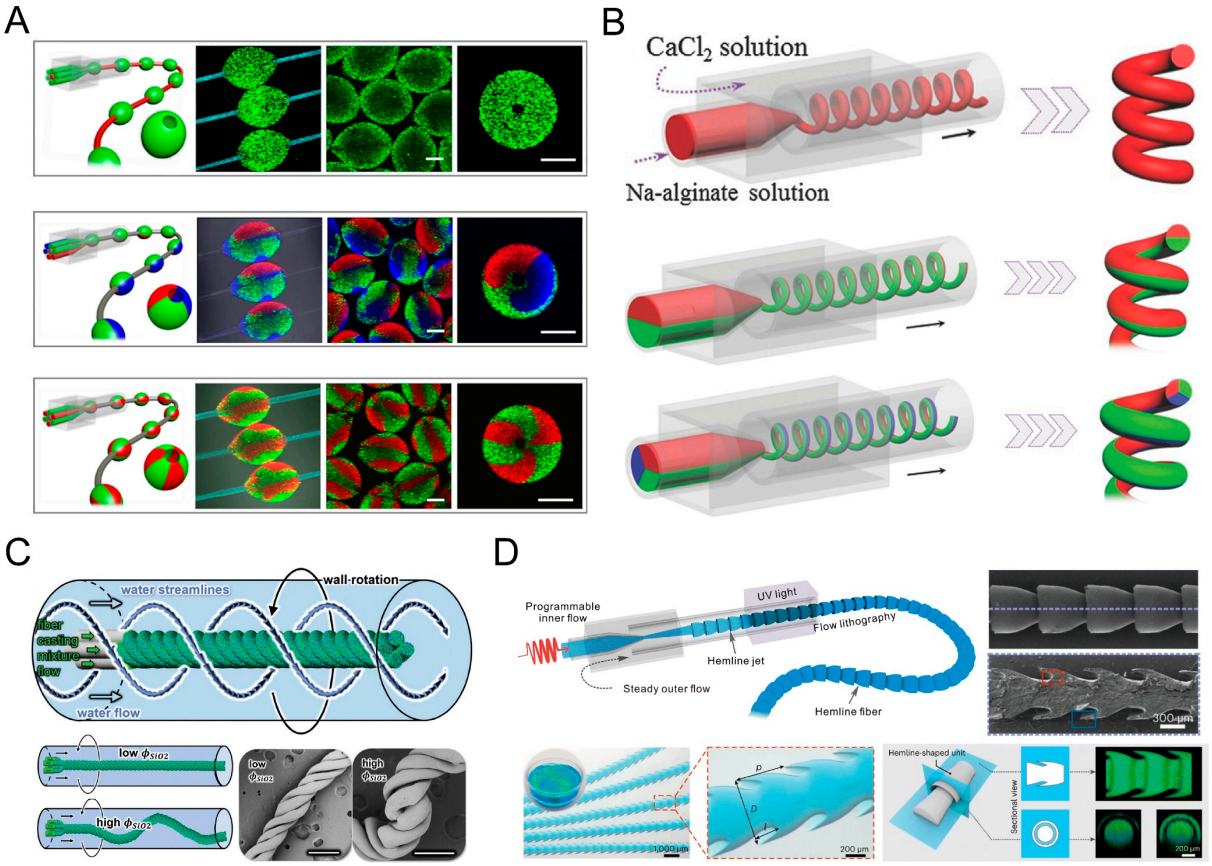


Figure 6: Axially varying jet-templated microfibers fabricated via microfluidics. (**A**) Spindle-knotted microfibers fabricated via emulsification-spinning synergy or piezoelectric vibration. Scale bars: 100 μm [65]. (**B**) Helical microfibers fabricated using coaxial capillaries with unbalanced fluidic friction [69]. (**C**) Twisted microfibers fabricated via centrifugal assembly using rotating outer capillaries. Scale bars: 200 μm [68]. (**D**) Hemline-shaped microfibers fabricated by programmable piezoelectric vibration [70].

5 Emerging Applications

Microfluidic template-derived soft matter, characterized by precise structural control, tunable functionalities, and excellent biocompatibility, has enabled diverse applications across multiple fields. By virtue of their tailored morphologies and spatially defined component distributions, these soft materials address critical needs in biomedical engineering, flexible electronics, soft robotics, and environmental science. These applications highlight the versatility of microfluidic templating in translating precise structural control into functional performance.

5.1 Biosensing and Bioanalysis

Microfluidically derived soft matter has enabled diverse advances in biosensing and bioanalysis, with specific platforms tailored to molecular quantification, mechanical sensing, and single-cell sequencing. Inverse opal microparticles, featuring periodically ordered porous frameworks and structural color characteristics, are particularly suitable for label-free biosensing. For example, microfluidic electrospray has been used to fabricate microcapsules encapsulating enzyme-immobilized inverse opal particles, which support stable enzyme cascade reactions for sensing (Fig. 7A) [109]. The hydrogel shell enhances enzyme stability against proteolysis while improving reaction efficiency, thereby enabling reliable detection. In addition, helical microfibers can serve as effective mechanical sensors for cardiomyocytes (Fig. 7B) [69]. By monitoring periodic changes in helical pitch synchronized with cardiomyocyte beating, these fibers can reflect real-time cellular activity and even estimate contraction force based on Hooke's law, providing a visual and low-instrumentation approach to cellular mechanical analysis.

Suspendable hydrogel nanovials facilitate high-throughput single-cell secretion analysis, including the screening of antigen-specific antibody-secreting cells and characterization of vascular endothelial growth factor A (VEGF-A) secretion by mesenchymal stromal cells (MSCs) [110]. These nanovials are compatible with fluorescence-activated cell sorting, enabling the enrichment of target cell populations while preserving cell viability for downstream single-cell RT-PCR or clonal expansion. Lab-on-a-particle technologies also include shape-encoded microparticles for multiplexed biosensing applications, such as human papillomavirus genotyping and cytokine panel detection, as well as particle-templated emulsions for digital PCR and digital ELISA [111]. These technologies enable the absolute quantification of low-abundance nucleic acids and proteins without the need for standard curves. Notably, secretion-encoded single-cell sequencing combines nanovials with single-cell RNA sequencing to correlate single-cell VEGF-A secretion with transcriptomic profiles, thereby identifying a vascular regenerative gene signature and enabling the enrichment of high-secreting MSC subpopulations via the interleukin-13 receptor subunit alpha 2 surface marker, ultimately enhancing cell therapy functionality (Fig. 7C) [112].

5.2 Drug/Cell Carrier and Tissue Biomimetic Scaffolds

Drug delivery systems based on microfluidic templates offer precise control over drug loading and release kinetics. Boston ivy-inspired disc-like adhesive microparticles, fabricated via droplet-templated colloidal crystal assembly, possess a unique nanostructured surface and adhesive hydrogel matrix that enhance adhesion to wet tissue surfaces (Fig. 7D) [113]. Loading dexamethasone into these particles prolongs drug retention in the inflamed colon, thereby improving therapeutic efficacy for ulcerative colitis. For gastric cancer treatment, suspended bubble microcapsules with a PLGA shell and gas core exploit their low density and hydrophobicity to resist gastric emptying and peristalsis, thereby prolonging local retention in the stomach [60]. Loaded with the chemotherapeutic drugs capecitabine and docetaxel, these microcapsules enable oral administration for localized tumor therapy, effectively inhibiting tumor proliferation and metastasis while reducing systemic side effects. For chronic kidney disease-associated hyperphosphatemia, biomimetic wrinkled prebiotic microspheres mimic intestinal microstructures to enhance intestinal retention and adsorb excess phosphate in the gastrointestinal tract. They also modulate the gut microbiota, thereby ameliorating vascular calcification and improving lipid metabolism [61].

In the field of cell delivery and tissue engineering, core–shell microfluidic bioprinting technology has enabled the construction of millimeter-thick 3D tissues using cell-laden core-shell microfibers (Fig. 7E) [114]. By encapsulating HepG2 cells within a soft extracellular matrix core, these scaffolds facilitate cell proliferation and extensive cell-cell interactions under dynamic culture conditions, resulting in enhanced albumin

secretion compared with 2D cultures and more closely mimicking the functional characteristics of native liver tissue. Biomimetic erythrocyte-like microparticles fabricated via microfluidic electrospray integrate hemoglobin, growth factors, and black phosphorus, enabling oxygen delivery and near-infrared-responsive (NIR) cargo release. Their discoid morphology enhances stacking stability at wound sites, promoting cell adhesion, angiogenesis, and extracellular matrix secretion, thereby accelerating tissue regeneration [47].

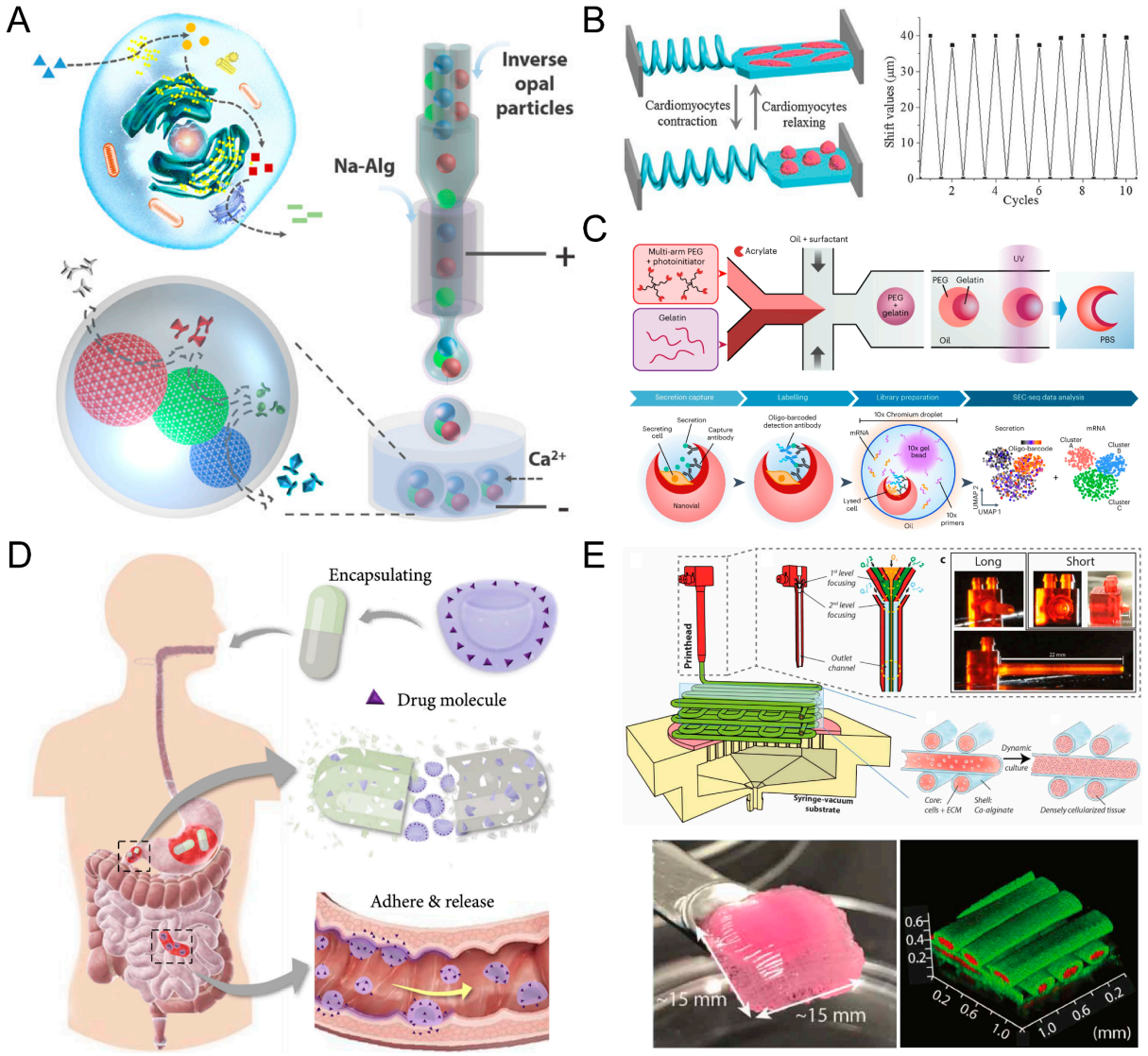


Figure 7: Biomedical applications of microfluidically derived soft matter. (**A**) Biosensing via enzyme-immobilized inverse opal particles encapsulated in electrospray microcapsules [109]. (**B**) Cardiomyocyte mechanical sensing using helical microfibers [69]. (**C**) Secretion-encoded single-cell sequencing using hydrogel nanovials [112]. (**D**) Colon-targeted drug delivery via Boston ivy-inspired disc-like adhesive microparticles [113]. (**E**) Liver tissue-mimetic scaffolds fabricated from cell-laden core–shell microfibers [114].

5.3 Flexible Electronics

Microfluidic technology has emerged as a key driving force in the advancement of flexible electronics, enabling the precise fabrication of functional microfibers, elastomers, and composite fabrics with tailored mechanical flexibility, electrical conductivity, and multifunctional integration. These devices have been

widely applied in wearable sensing, smart textiles, and flexible circuits, enabling the real-time detection of human motion, biological signals, and environmental stimuli.

Liquid metal (LM) droplet-based elastomers fabricated via revolving microfluidics exhibit stable electrical performance and self-healing properties, enabling sensitive monitoring of wrist and leg movements and grip forces (Fig. 8A) [115]. LM droplet elastomers also enable programmable patterning of conductive pathways, forming self-healing circuits that recover conductivity after cutting and heating and supporting LED arrays and parallel circuits with high tolerance to bending. In addition, tough hydrogel microfibers and nanofibers with nanoscale skin-like structures (NSFs) can be used to detect human motions, such as walking, jumping, and hand clapping, as well as bio-signals, such as writing patterns. NSF-based triboelectric nanogenerators (TENGs) harvest mechanical deformation and transduce it into electrical outputs, thereby supporting self-powered sensing. Core–shell structured conductive microfibers, such as PEDOT:PSS-core–ALG-shell fibers fabricated via multiflow microfluidics, provide tunable electrical conductivity and mechanical properties for bending detection (Fig. 8B) [72]. These microfibers can be woven into textiles or integrated into flexible films, exhibiting sensitive resistance responses to small deformations, which are crucial for detecting subtle movements in human-machine interaction. MXene-based hydrogel microfibers, characterized by superelasticity and electrical conductivity, can serve as electronic skin for joint monitoring, reliably capturing movements of the fingers, elbows, knees, and waist by converting mechanical deformation into changes in electrical resistance [73]. Shear-flow-induced GO-coated microfibers integrate thermal and motion-sensing capabilities, functioning as gesture indicators for recognizing combinations of finger bending and sign language.

5.4 Soft Robotics and Actuators

Beyond these applications, SR microfibers and microparticles can also function as soft actuators, undergoing controlled deformation responsive to temperature, light, and magnetic fields. For example, helical microfibers embedded with magnetic nanoparticles respond to magnetic fields, exhibiting stretching and contraction behaviors that mimic microsprings. These fibers can be integrated into soft robots for the precise manipulation of micro-objects, such as single cells and droplets [116]. Shape-memory hydrogel microfibers prepared via microfluidic photopolymerization undergo reversible shape changes in response to temperature variations, enabling the design of soft robotic arms for grasping and releasing tasks. Helical micromotors prepared via microfluidic lithography or spinning mimic bacterial flagella and achieve controllable locomotion through magnetic actuation or chemical catalysis, with potential applications in targeted drug delivery, cell transportation, and biofilm eradication (Fig. 8C) [23].

Microfluidically derived microcapsules and microtubes can serve as fluidic components in soft robots. Flexible liquid-diode microtubes fabricated via multimodal microfluidics can regulate unidirectional liquid flow, functioning as microvalves in soft robotic pumps [117]. Janus hydrogel microrobots, with bioactive ion gradients, combine locomotion and therapeutic functions (Fig. 8D) [118]. These microrobots can be used for the targeted delivery of growth factors to promote regeneration of the tendon–bone interface, demonstrating the potential of soft matter in biomedical robotics. Sun et al. demonstrated that core–shell LM–liquid crystal elastomer (LCE) fibers can function as efficient electrothermal actuators for load-lifting applications by leveraging the conductive LM core to generate Joule heating and trigger a phase transition in the LCE shell [119]. Upon application of an electrical voltage, the fibers contract along the axial direction to lift external loads and relax to their original state after the voltage is removed, demonstrating reliable and reversible actuation (Fig. 8E).

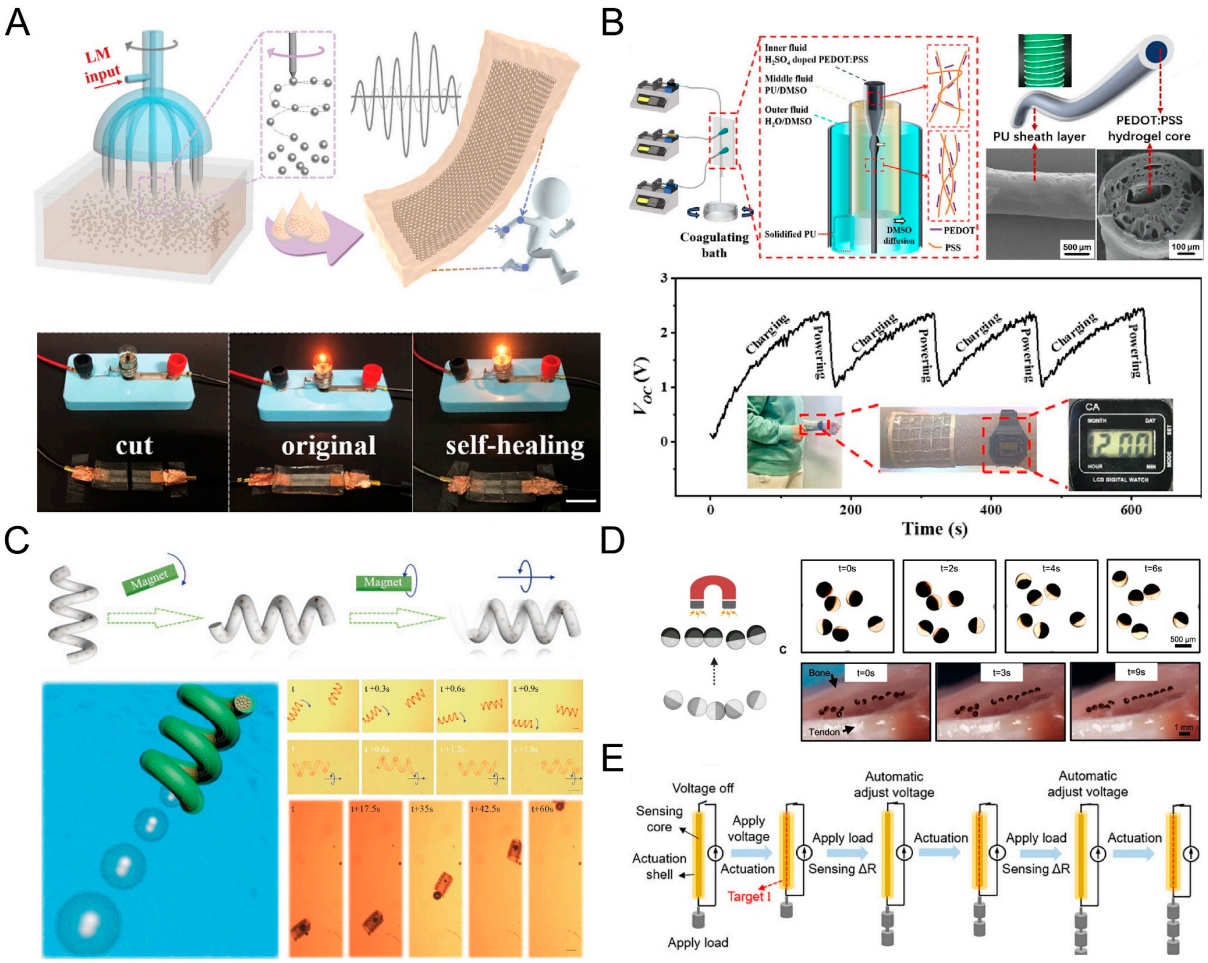


Figure 8: Applications of microfluidically derived soft matter in flexible electronics and soft robotics. (**A**) Wearable sensing using LM droplet-based elastomers. Scale bar: 1 cm [115]. (**B**) Bending detection using PEDOT:PSS-core–ALG-shell conductive microfibers [72]. (**C**) Targeted drug delivery via magnetic helical micromotors. Scale bars: 250 μm (upper two rows) and 350 μm (bottom row) [23]. (**D**) Tendon–bone interface regeneration using magnetically controlled Janus hydrogel microrobots [118]. (**E**) Microfiber actuators for load lifting [119].

5.5 Other Applications

Microfluidic-derived functional materials, with precisely tailored structures and stimuli responsiveness, have expanded into diverse emerging applications beyond biomedical and electronic fields, including high-performance energy storage, emulsion stabilization, pollutant remediation, and liquid directional transport. These examples are included to further illustrate the broad structure–function versatility of microfluidic templating and to provide complementary design insights for the development of biomedical soft materials.

For energy-storage applications, an integrated microfluidic spinning and chemical synthesis process was used to directly construct nickel molybdate–porous graphene carbonene fiber ($NiMoO_4$/PGCF) hybrids, addressing the issues of graphene restacking and nonuniform hybridization. The resulting composite fibers exhibit exceptional electrochemical performance, including ultrahigh areal capacitance in both a three-electrode system and solid-state supercapacitors, as well as superior energy density and long-term cycling stability, with minimal capacitance loss after prolonged charge-discharge cycling. In practical applications,

these supercapacitors can independently power toy windmills and function as supercapacitive controllers coupled with triodes to regulate the unmanned aircraft takeoff (Fig. 9A) [75].

As Pickering emulsifiers, amphiphilic Janus microgels synthesized via microfluidic droplet templating are highly effective for stabilizing oil–water emulsions. These microgels feature spatially distinct hydrophilic (poly(ethylene glycol) diacrylate) and hydrophobic (poly(propylene glycol) diacrylate) domains that selectively swell in their corresponding solvents, enabling irreversible adsorption at the oil–water interface and providing long-term emulsion stability (Fig. 9B) [120]. Temperature-responsive variants further enable on-demand emulsion destabilization through thermal stimulation, with applications in biocatalysis, fuel production, and controlled cargo release. Compared with conventional surfactants, these microgels offer enhanced stability and stimulus responsiveness.

For pollutant remediation, microfluidically derived micromotors and anisotropic particles enable active and efficient contaminant removal. Magnetic graphene-based helical micromotors, actuated by rotating magnetic fields, rapidly adsorb organic dyes and heavy metals, while Ag-modified variants can eliminate pathogenic bacteria via mechanical disruption and reactive oxygen species (ROS) generation [121]. Bioinspired jellyfish-like microparticles, integrated with GO/NIPAM and Fe_3O_4 nanoparticles, exhibit NIR and magnetic responsiveness, enhancing contact with pollutants through controlled motion and thereby improving adsorption efficiency (Fig. 9C) [62]. Additionally, Fe_2O_3 helical micromotors can eradicate bacterial biofilms in confined spaces through the synergistic effects of mechanical forces and ROS-mediated catalysis, addressing biofilm-associated infections [122].

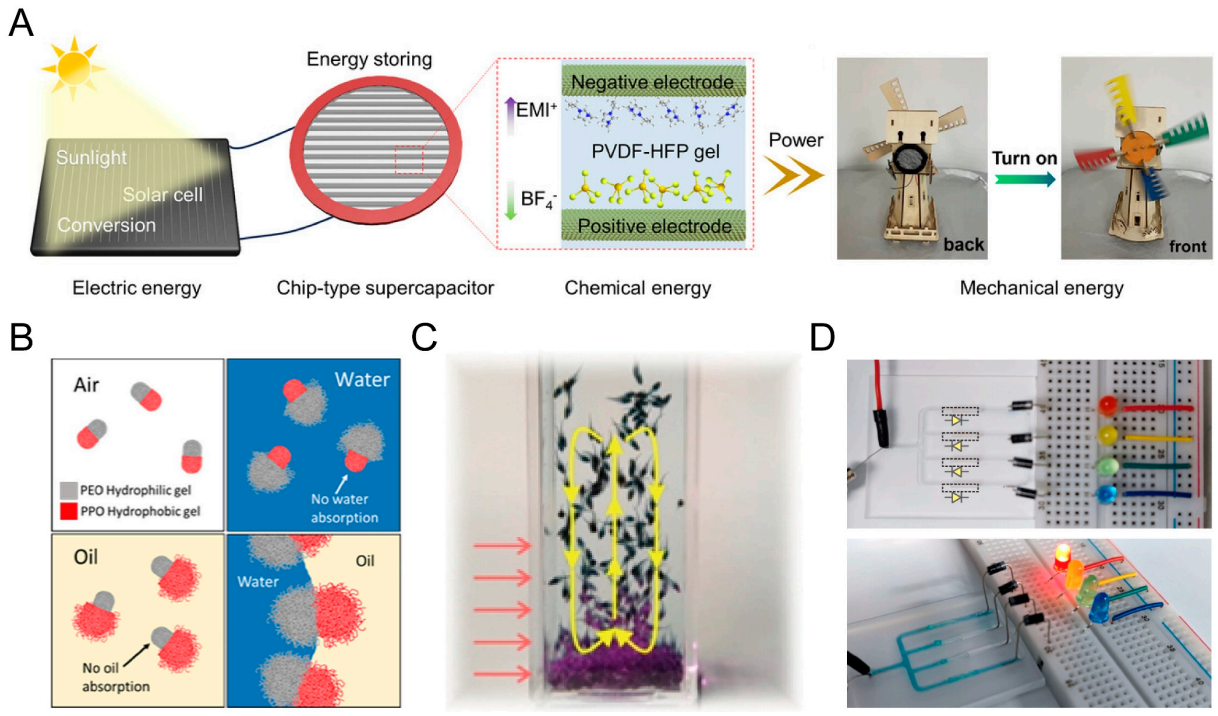


Figure 9: Other applications of microfluidically derived soft matter. (**A**) Energy storage using $NiMoO_4$–PGCF composite fibers fabricated via the microfluidic-spinning-chemistry strategy [75]. (**B**) Oil–water emulsion stabilization using amphiphilic Janus microgels [120]. (**C**) Pollutant remediation using NIR–magnetic-responsive jellyfish-like microparticles [62]. (**D**) Directional liquid transport via hemline-shaped microfibers and corrugated liquid-diode microtubes [108].

Liquid directional transport can be achieved via microfluidic-fabricated fibers and microtubes with asymmetric structures. Hemline-shaped microfibers use periodic axial microcavities to direct liquid flow across hydrophilic and hydrophobic surfaces, even without a supporting substrate, enabling 3D path transport, water extraction, and oil–water separation [70]. Flexible liquid-diode microtubes with corrugated inner walls further enable directional liquid transport in confined spaces through unbalanced Laplace pressure, allowing antigravity transport and integration into fluidic-electronic circuits for logic operations. These capabilities expand the scope of open microfluidics and confined-space fluid control (Fig. 9D) [108].

6 Conclusion

This review highlights the unique capability of microfluidics to construct soft matter with precisely regulated architectures, compositions, and spatial organization. By exploiting controllable fluidic interfaces, microfluidic droplets and jets provide versatile and programmable templates for translating dynamic fluid structures into stable soft materials. The ability to manipulate structural features across multiple length scales, from overall morphology to internal compartmentalization and component distribution, has enabled the development of soft matter with tailored properties and functions. These advances have expanded the application potential of microfluidically fabricated materials across diverse fields, including biomedical engineering, flexible electronics, soft robotics, and environmental technologies.

Despite significant progress, further development of microfluidic template-based soft matter requires addressing several fundamental and technological challenges. First, future efforts should move beyond the fabrication of static structures toward the development of adaptive and dynamic soft materials with biomimetic behaviors. Integrating responsive chemical components, dynamic assemblies, and programmable interfaces into microfluidic templates may enable materials capable of undergoing controlled structural evolution in response to external stimuli, thereby more closely recapitulating the adaptability of biological systems. Second, improving the robustness and functionality of these materials under complex operating conditions remains essential. For practical applications, microfluidically fabricated soft matter must maintain structural integrity and functional performance under conditions involving mechanical deformation, chemical fluctuations, and biological complexity. Third, establishing deeper structure–function relationships across multiple length scales will be critical for rational material design. Integrating microfluidic fabrication with advanced characterization, computational modeling, and emerging manufacturing technologies, such as high-resolution additive manufacturing and *in situ* assembly strategies, may provide new opportunities to elucidate and engineer complex hierarchical architectures.

Overall, microfluidic templating is expected to evolve from a strategy for fabricating precisely structured soft materials into a versatile approach for integrating structural complexity with functional diversity. Continued advances in fluidic control, material design, and bioinspired engineering will enable the development of soft matter systems with enhanced adaptability and application-specific functionalities. Such developments may open new possibilities in fields ranging from advanced biomedical technologies to sustainable materials and responsive devices. Ultimately, the integration of precise microscale organization with functional material design will continue to drive the evolution of microfluidic templating as a powerful platform for constructing next-generation soft matter.

Acknowledgement: This work was supported by Shenzhen Medical Research Fund (B2401006).

Funding Statement: This research was funded by Shenzhen Medical Research Fund (B2401006) and the APC was funded by Shenzhen Medical Research Fund (B2401006).

Author Contributions: The authors confirm contribution to the paper as follows: conceptualization, Zhonglin Fang and Chong Wang; investigation, Zhonglin Fang; writing—original draft preparation, Zhonglin Fang; writing—review and editing, Zhonglin Fang and Chong Wang; supervision, Chong Wang. All authors reviewed and approved the final version of the manuscript.

Availability of Data and Materials: Not applicable.

Ethics Approval: Not applicable.

Conflicts of Interest: The authors declare no conflict of interest.

References

1. Weitz DA. Soft materials evolution and revolution. Nat Mater. 2022;21(9):986–8. [CrossRef].
2. Li X, Liu J, Zhang X. Pressure/temperature dual-responsive cellulose nanocrystal hydrogels for on-demand schemochrome patterning. Adv Funct Mater. 2023;33(47):2306208. [CrossRef].
3. Sun X, He Z, Zou F, Tian H. Temperature-controlled sinking delivery of thermostable alkyl substituted benzimidazole by sodium alginate polymer gel network for efficient inhibition of carbon steel corrosion in acid oilfield solution. Chem Eng J. 2025;513:162912. [CrossRef].
4. An D, Warning A, Yancey KG, Chang CT, Kern VR, Datta AK, et al. Mass production of shaped particles through *Vortex ring* freezing. Nat Commun. 2016;7:12401. [CrossRef].
5. Zheng Y, Oz Y, Gu Y, Ahamad N, Shariati K, Chevalier J, et al. Rational design of polymeric micelles for targeted therapeutic delivery. Nano Today. 2024;55:102147. [CrossRef].
6. Araújo NAM, Janssen LMC, Barois T, Boffetta G, Cohen I, Corbetta A, et al. Steering self-organisation through confinement. Soft Matter. 2023;19(9):1695–704. [CrossRef].
7. Fang Y, Shi J, Liang J, Ma D, Wang H. Water-regulated viscosity-plasticity phase transitions in a peptide self-assembled muscle-like hydrogel. Nat Commun. 2025;16(1):1058. [CrossRef].
8. Yu M, Song W, Tian F, Dai Z, Zhu Q, Ahmad E, et al. Temperature- and rigidity-mediated rapid transport of lipid nanovesicles in hydrogels. Proc Natl Acad Sci U S A. 2019;116(12):5362–9. [CrossRef].
9. Liu Z, Li YR, Yang Y, Zhu Y, Yuan W, Hoffman T, et al. Viscoelastic synthetic antigen-presenting cells for augmenting the potency of cancer therapies. Nat Biomed Eng. 2024;8(12):1615–33. [CrossRef].
10. Fu X, Cai J, Zhang X, Li WD, Ge H, Hu Y. Top-down fabrication of shape-controlled, monodisperse nanoparticles for biomedical applications. Adv Drug Deliv Rev. 2018;132:169–87. [CrossRef].
11. Choi S, Lee KY, Kim SL, MacQueen LA, Chang H, Zimmerman JF, et al. Fibre-infused gel scaffolds guide cardiomyocyte alignment in 3D-printed ventricles. Nat Mater. 2023;22(8):1039–46. [CrossRef].
12. Cai L, Luo Z, Chen H, Zhao Y. Lithographic microneedle-motors from multimodal microfluidics for cargo delivery. Small. 2023;19(12):2206108. [CrossRef].
13. Levato R, Dudaryeva O, Garciamendez-Mijares CE, Kirkpatrick BE, Rizzo R, Schimelman J, et al. Light-based vat-polymerization bioprinting. Nat Rev Methods Prim. 2023;3:47. [CrossRef].
14. Jian G, Li D, Ying Q, Chen X, Zhai Q, Wang S, et al. Dual photo-enhanced interpenetrating network hydrogel with biophysical and biochemical signals for infected bone defect healing. Adv Healthc Mater. 2023;12(25):e2300469. [CrossRef].
15. Song N, Tian F, Zou Y, Yu Z. Self-assembly in living cells: bottom-up syntheses in natural factory. ACS Appl Mater Interfaces. 2024;16(35):45821–9. [CrossRef].
16. Truby RL, Lewis JA. Printing soft matter in three dimensions. Nature. 2016;540(7633):371–8. [CrossRef].
17. Xu W, Jambhulkar S, Ravichandran D, Zhu Y, Kakarla M, Nian Q, et al. 3D printing-enabled nanoparticle alignment: a review of mechanisms and applications. Small. 2021;17(45):2100817. [CrossRef].
18. Li W, Zhang L, Ge X, Xu B, Zhang W, Qu L, et al. Microfluidic fabrication of microparticles for biomedical applications. Chem Soc Rev. 2018;47(15):5646–83. [CrossRef].
19. Wu R, Kim T. Review of microfluidic approaches for fabricating intelligent fiber devices: importance of shape characteristics. Lab Chip. 2021;21(7):1217–40. [CrossRef].

20. Kaminski TS, Garstecki P. Controlled droplet microfluidic systems for multistep chemical and biological assays. Chem Soc Rev. 2017;46(20):6210–26. [CrossRef].
21. Shang L, Cheng Y, Zhao Y. Emerging droplet microfluidics. Chem Rev. 2017;117(12):7964–8040. [CrossRef].
22. Onoe H, Okitsu T, Itou A, Kato-Negishi M, Gojo R, Kiriya D, et al. Metre-long cell-laden microfibres exhibit tissue morphologies and functions. Nat Mater. 2013;12(6):584–90. [CrossRef].
23. Yu Y, Shang L, Gao W, Zhao Z, Wang H, Zhao Y. Microfluidic lithography of bioinspired helical micromotors. Angew Chem Int Ed. 2017;56(40):12127–31. [CrossRef].
24. Maeki M, Uno S, Niwa A, Okada Y, Tokeshi M. Microfluidic technologies and devices for lipid nanoparticle-based RNA delivery. J Control Release. 2022;344:80–96. [CrossRef].
25. Yan W, Li X, Zhao D, Xie M, Li T, Qian L, et al. Advanced strategies in high-throughput droplet screening for enzyme engineering. Biosens Bioelectron. 2024;248:115972. [CrossRef].
26. Wu L, Guo Z, Liu W. Surface behaviors of droplet manipulation in microfluidics devices. Adv Colloid Interface Sci. 2022;308:102770. [CrossRef].
27. Zhu Z, Chen T, Huang F, Wang S, Zhu P, Xu RX, et al. Free-boundary microfluidic platform for advanced materials manufacturing and applications. Adv Mater. 2024;36(7):2304840. [CrossRef].
28. Dinh T, Cubaud T. Role of interfacial tension on viscous multiphase flows in coaxial microfluidic channels. Langmuir. 2021;37(24):7420–9. [CrossRef].
29. Ma L, Zhao X, Hou J, Huang L, Yao Y, Ding Z, et al. Droplet microfluidic devices: working principles, fabrication methods, and scale-up applications. Small Methods. 2024;8(8):e2301406. [CrossRef].
30. Li XB, Li FC, Yang JC, Kinoshita H, Oishi M, Oshima M. Study on the mechanism of droplet formation in T-junction microchannel. Chem Eng Sci. 2012;69(1):340–51. [CrossRef].
31. Fu T, Wu Y, Ma Y, Li HZ. Droplet formation and breakup dynamics in microfluidic flow-focusing devices: from dripping to jetting. Chem Eng Sci. 2012;84:207–17. [CrossRef].
32. Wang C, Zhang Z, Wang Q, Wang J, Shang L. Aqueous two-phase emulsions toward biologically relevant applications. Trends Chem. 2023;5(1):61–75. [CrossRef].
33. Saleem MS, Chan TTK, Versluis M, Krug D, Lajoinie G. Additive manufacturing of 3D flow-focusing millifluidics for the production of curable microdroplets. RSC Adv. 2024;14(53):39276–84. [CrossRef].
34. Atefi E, Mann JA Jr, Tavana H. Ultralow interfacial tensions of aqueous two-phase systems measured using drop shape. Langmuir. 2014;30(32):9691–9. [CrossRef].
35. Mastiani M, Seo S, Mosavati B, Kim M. High-throughput aqueous two-phase system droplet generation by oil-free passive microfluidics. ACS Omega. 2018;3(8):9296–302. [CrossRef].
36. Geschiere SD, Ziemecka I, van Steijn V, Koper GJM, Esch JHV, Kreutzer MT. Slow growth of the Rayleigh-Plateau instability in aqueous two phase systems. Biomicrofluidics. 2012;6(2):22007–2200711. [CrossRef].
37. Cheung Shum H, Varnell J, Weitz DA. Microfluidic fabrication of water-in-water (w/w) jets and emulsions. Biomicrofluidics. 2012;6(1):12808–128089. [CrossRef].
38. Zhu K, Yu Y, Cheng Y, Tian C, Zhao G, Zhao Y. All-aqueous-phase microfluidics for cell encapsulation. ACS Appl Mater Interfaces. 2019;11(5):4826–32. [CrossRef].
39. Mak SY, Chao Y, Rahman S, Shum HC. Droplet formation by rupture of vibration-induced interfacial fingers. Langmuir. 2018;34(3):926–32. [CrossRef].
40. Chao Y, Shum HC. Emerging aqueous two-phase systems: from fundamentals of interfaces to biomedical applications. Chem Soc Rev. 2020;49(1):114–42. [CrossRef].
41. Cheng Y, Zhu C, Xie Z, Gu H, Tian T, Zhao Y, et al. Anisotropic colloidal crystal particles from microfluidics. J Colloid Interface Sci. 2014;421:64–70. [CrossRef].
42. Krüger AJD, Bakirman O, Guerzoni LPB, Jans A, Gehlen DB, Rommel D, et al. Compartmentalized jet polymerization as a high-resolution process to continuously produce anisometric microgel rods with adjustable size and stiffness. Adv Mater. 2019;31(49):1903668. [CrossRef].
43. Yang Y, Vagin SI, Rieger B, Destgeer G. Fabrication of crescent shaped microparticles for particle templated droplet formation. Macromol Rapid Commun. 2024;45(13):2300721. [CrossRef].
44. Geng YH, Ge XH, Zhang SB, Zhou YW, Wang ZQ, Chen J, et al. Microfluidic preparation of flexible micro-grippers with precise delivery function. Lab Chip. 2018;18(13):1838–43. [CrossRef].

45. Zhou C, Man J, Yu H, Xia H, Man L, Qi B, et al. Fabrication of crescent-shaped ceramic microparticles based on single emulsion microfluidics. Ceram Int. 2021;47(8):10866–72. [CrossRef].
46. Nisisako T, Ando T, Hatsuzawa T. Capillary-assisted fabrication of biconcave polymeric microlenses from microfluidic ternary emulsion droplets. Small. 2014;10(24):5116–25. [CrossRef].
47. Luo Z, Cai L, Chen H, Chen G, Zhao Y. Biomimetic erythrocyte-like particles from microfluidic electrospray for tissue engineering. Engineering. 2024;40:78–86. [CrossRef].
48. Cai L, Zhao C, Chen H, Fan L, Zhao Y, Qian X, et al. Suction-cup-inspired adhesive micromotors for drug delivery. Adv Sci. 2022;9:2103384. [CrossRef].
49. Wei Y, Zhang F, Li J, Qi Z, Wang JH, Wang Z. Composition tuning of semi-open cell carriers *via* phase freeze-shrink self-molding. ACS Nano. 2024;18(39):26872–81. [CrossRef].
50. Wang Y, Shang L, Chen G, Shao C, Liu Y, Lu P, et al. Pollen-inspired microparticles with strong adhesion for drug delivery. Appl Mater Today. 2018;13:303–9. [CrossRef].
51. Zheng Y, Wu Z, Hou Y, Li N, Zhang Q, Lin JM. Microfluidic engineering of crater-terrain hydrogel microparticles: toward novel cell carriers. ACS Appl Mater Interfaces. 2023;15(6):7833–40. [CrossRef].
52. Wang L, Ding X, Fan L, Filppula AM, Li Q, Zhang H, et al. Self-healing dynamic hydrogel microparticles with structural color for wound management. Nano Micro Lett. 2024;16(1):232. [CrossRef].
53. Chen J, Li P, An R, Cai A, Wang K, Zhang Z, et al. Droplet microfluidics-assisted fabrication of Fe-alginate microgels with complex morphology: effect of the composition of droplets. Lab Chip. 2025;25(13):3270–86. [CrossRef].
54. Min NG, Kim B, Lee TY, Kim D, Lee DC, Kim SH. Anisotropic microparticles created by phase separation of polymer blends confined in monodisperse emulsion drops. Langmuir. 2015;31(3):937–43. [CrossRef].
55. Zhang L, Chen K, Zhang H, Pang B, Choi CH, Mao AS, et al. Microfluidic templated multicompartment microgels for 3D encapsulation and pairing of single cells. Small. 2018;14(9):1702955. [CrossRef].
56. Wu Z, Zheng Y, Lin L, Lin Y, Xie T, Liao W, et al. Open aerosol microfluidics enable orthogonal compartmentalized functionalization of hydrogel particles. Matter. 2024;7(10):3645–57. [CrossRef].
57. Huang D, Wang J, Nie M, Chen G, Zhao Y. Pollen-inspired adhesive multilobe microparticles from microfluidics for intestinal drug delivery. Adv Mater. 2023;35(28):e2301192. [CrossRef].
58. Zhong J, Zhang Q, Kuang G, Xia J, Shang L. Multicomponent microspheres with spatiotemporal drug release for post-surgical liver cancer treatment and liver regeneration. Chem Eng J. 2023;455:140585. [CrossRef].
59. Wang H, Cai L, Zhang D, Shang L, Zhao Y. Responsive Janus structural color hydrogel micromotors for label-free multiplex assays. Research. 2021;2021:9829068. [CrossRef].
60. Chen X, Liang D, Sun W, Shou X, Shang L, Shen X. Suspended bubble microcapsule delivery systems from droplet microfluidic technology for the local treatment of gastric cancer. Chem Eng J. 2023;458:141428. [CrossRef].
61. Hu B, Wang Y, Yu L, Cao L, Liu S, Zhong L, et al. Biomimetic wrinkled prebiotic microspheres with enhanced intestinal retention for hyperphosphatemia and vascular calcification. Sci Adv. 2025;11(3):eads5286. [CrossRef].
62. Yang C, Yu Y, Zhao Y, Shang L. Bioinspired jellyfish microparticles from microfluidics. Research. 2023;6:0034. [CrossRef].
63. Wei D, Sun J, Bolderson J, Zhong M, Dalby MJ, Cusack M, et al. Continuous fabrication and assembly of spatial cell-laden fibers for a tissue-like construct *via* a photolithographic-based microfluidic chip. ACS Appl Mater Interfaces. 2017;9(17):14606–17. [CrossRef].
64. Wang X, Yu Y, Yang C, Shao C, Shi K, Shang L, et al. Microfluidic 3D printing responsive scaffolds with biomimetic enrichment channels for bone regeneration. Adv Funct Mater. 2022;32(7):2111909. [CrossRef].
65. Yu Y, Shang L, Guo J, Wang J, Zhao Y. Design of capillary microfluidics for spinning cell-laden microfibers. Nat Protoc. 2018;13(11):2557–79. [CrossRef].
66. Wu Z, Wang J, Zhao Z, Yu Y, Shang L, Zhao Y. Microfluidic generation of bioinspired spindle-knotted graphene microfibers for oil absorption. Chemphyschem. 2018;19(16):1990–4. [CrossRef].
67. Yang C, Yu Y, Wang X, Zu Y, Zhao Y, Shang L. Bioinspired stimuli-responsive spindle-knotted fibers for droplet manipulation. Chem Eng J. 2023;451:138669. [CrossRef].
68. Kharal SP, Haase MF. Centrifugal assembly of helical bijel fibers for pH responsive composite hydrogels. Small. 2022;18(11):2106826. [CrossRef].

69. Yu Y, Fu F, Shang L, Cheng Y, Gu Z, Zhao Y. Bioinspired helical microfibers from microfluidics. Adv Mater. 2017;29(18):1605765. [CrossRef].
70. Yang C, Yu Y, Shang L, Zhao Y. Flexible hemline-shaped microfibers for liquid transport. Nat Chem Eng. 2024;1(1):87–96. [CrossRef].
71. Takeuchi N, Nakajima S, Yoshida K, Kawano R, Hori Y, Onoe H. Microfiber-shaped programmable materials with stimuli-responsive hydrogel. Soft Robot. 2022;9(1):89–97. [CrossRef].
72. Chen N, Wei W, Ning N, Wu H, Tian M. All-Polymeric stretchable conductive fiber with versatile intelligent wearable applications *via* microfluidic spinning technology. Chem Eng J. 2024;487:150741. [CrossRef].
73. Guo J, Yu Y, Zhang H, Sun L, Zhao Y. Elastic MXene hydrogel microfiber-derived electronic skin for joint monitoring. ACS Appl Mater Interfaces. 2021;13(40):47800–6. [CrossRef].
74. Yu Y, Guo J, Zhang H, Wang X, Yang C, Zhao Y. Shear-flow-induced graphene coating microfibers from microfluidic spinning. Innovation. 2022;3(2):100209. [CrossRef].
75. Guo J, Zhang Y, Zhou L, Hou W, Wang J, Zhu L, et al. Microfluidic-spinning-chemistry strategy toward *in-situ* generation of high-performance nickel molybdate/porous graphene carbonene fiber-based supercapacitors. Adv Energy Mater. 2025;15(34):2501418. [CrossRef].
76. Jiang W, Li M, Chen Z, Leong KW. Cell-laden microfluidic microgels for tissue regeneration. Lab Chip. 2016;16(23):4482–506. [CrossRef].
77. Amirifar L, Besanjideh M, Nasiri R, Shamloo A, Nasrollahi F, de Barros NR, et al. Droplet-based microfluidics in biomedical applications. Biofabrication. 2022;14(2):022001. [CrossRef].
78. Cai L, Li N, Zhang Y, Gu H, Zhu Y. Microfluidics-derived microcarrier systems for oral delivery. Biomed Technol. 2023;1:30–8. [CrossRef].
79. Fang Z, Yang X, Wang C, Shang L. Microfluidics-based microcarriers for live-cell delivery. Adv Sci. 2025;12(18):2414410. [CrossRef].
80. Ramirez-Calderon G, Susapto HH, Hauser CAE. Delivery of endothelial cell-laden microgel elicits angiogenesis in self-assembling ultrashort peptide hydrogels *in vitro*. ACS Appl Mater Interfaces. 2021;13(25):29281–92. [CrossRef].
81. Huang J, Fu D, Wu X, Li Y, Zheng B, Liu Z, et al. One-step generation of core-shell biomimetic microspheres encapsulating double-layer cells using microfluidics for hair regeneration. Biofabrication. 2023;15(2):025007. [CrossRef].
82. Chen G, Wang F, Nie M, Zhang H, Zhang H, Zhao Y. Roe-inspired stem cell microcapsules for inflammatory bowel disease treatment. Proc Natl Acad Sci U S A. 2021;118(43):e2112704118. [CrossRef].
83. Qazi TH, Wu J, Muir VG, Weintraub S, Gullbrand SE, Lee D, et al. Anisotropic rod-shaped particles influence injectable granular hydrogel properties and cell invasion. Adv Mater. 2022;34(12):e2109194. [CrossRef].
84. Xu Y, Qi R, Zhu H, Li B, Shen Y, Krainer G, et al. Liquid–liquid phase-separated systems from reversible gel–sol transition of protein microgels. Adv Mater. 2021;33(33):2008670. [CrossRef].
85. Kittel Y, Guerzoni LPB, Itzin C, Rommel D, Mork M, Bastard C, et al. Varying the stiffness and diffusivity of rod-shaped microgels independently through their molecular building blocks. Angew Chem Int Ed. 2023;62(44):e202309779. [CrossRef].
86. Rommel D, Mork M, Vedaraman S, Bastard C, Guerzoni LPB, Kittel Y, et al. Functionalized microgel rods interlinked into soft macroporous structures for 3D cell culture. Adv Sci. 2022;9(10):e2103554. [CrossRef].
87. Cai QW, Ju XJ, Chen C, Faraj Y, Jia ZH, Hu JQ, et al. Fabrication and flow characteristics of monodisperse bullet-shaped microparticles with controllable structures. Chem Eng J. 2019;370:925–37. [CrossRef].
88. Tang RC, Shang L, Scumpia PO, di Carlo D. Injectable microporous annealed crescent-shaped (MAC) particle hydrogel scaffold for enhanced cell infiltration. Adv Healthc Mater. 2024;13(25):e2302477. [CrossRef].
89. Chen L, Du Y, Rao S, Shi Q, Cui Y, Zhou L, et al. Accurate and microfluidics-free digital nucleic acid quantification with crescent microbeads-templated emulsions. ACS Sens. 2025;10(9):6645–55. [CrossRef].
90. Keller S, Dekkers R, Hu GX, Tollemeto M, Morosini M, Keskin A, et al. A simple microfluidic tool to design anisotropic microgels. React Funct Polym. 2021;167:105012. [CrossRef].
91. Cui Y, Zhang H, Wang J. Preparation of ethyl cellulose particles with different morphologies through microfluidics. Soft Matter. 2022;18(7):1455–62. [CrossRef].

92. Yang J, Ma M, Zhao C, Chen Y, Sun J, Sun Y, et al. Janus NPs@MOFs-based nanosensors for real-time visual monitoring and enhanced therapy of colon cancer. Chem Eng J. 2025;508:161091. [CrossRef].
93. Luo R, Liu J, Cheng Q, Shionoya M, Gao C, Wang R. Oral microsphere formulation of M2 macrophage-mimetic Janus nanomotor for targeted therapy of ulcerative colitis. Sci Adv. 2024;10(26):eado6798. [CrossRef].
94. Yang L, Yang W, Xu W, Zhao Y, Shang L. Bio-inspired Janus microcarriers with sequential actives release for bone regeneration. Chem Eng J. 2023;476:146797. [CrossRef].
95. Shang L, Shangguan F, Cheng Y, Lu J, Xie Z, Zhao Y, et al. Microfluidic generation of magnetoresponsive Janus photonic crystal particles. Nanoscale. 2013;5(20):9553–7. [CrossRef].
96. Wu Q, Yang C, Liu G, Xu W, Zhu Z, Si T, et al. Multiplex coaxial flow focusing for producing multicompartment Janus microcapsules with tunable material compositions and structural characteristics. Lab Chip. 2017;17(18):3168–75. [CrossRef].
97. Wu Z, Zheng Y, Lin L, Lin Y, Xie T, Lin J, et al. Fabrication and performance of bubble-containing multicompartmental particles: novel self-orienting carriers. Small. 2024;20(17):e2306814. [CrossRef].
98. Lin Y, Wu Z, Zheng Y, Wang X, Lin JM, Hou Y, et al. Microfluidic engineering of addressable multicompartmental microspheres for multicellular systems. Anal Chem. 2024;96:13762–7. [CrossRef].
99. Wu Z, Zheng Y, Lin L, Xing G, Xie T, Lin J, et al. Construction of multiplexed assays on single anisotropic particles using microfluidics. ACS Cent Sci. 2025;11(2):294–301. [CrossRef].
100. Cheng Y, Yu Y, Fu F, Wang J, Shang L, Gu Z, et al. Controlled fabrication of bioactive microfibers for creating tissue constructs using microfluidic techniques. ACS Appl Mater Interfaces. 2016;8(2):1080–6. [CrossRef].
101. Zhao G, Wu T, Wang R, Li Z, Yang Q, Wang L, et al. Hydrogel-assisted microfluidic spinning of stretchable fibers *via* fluidic and interfacial self-adaptations. Sci Adv. 2023;9(42):eadj5407. [CrossRef].
102. Yu Y, Wei W, Wang Y, Xu C, Guo Y, Qin J. Simple spinning of heterogeneous hollow microfibers on chip. Adv Mater. 2016;28(31):6649–55. [CrossRef].
103. Abrishamkar A, Nilghaz A, Saadatmand M, Naeimirad M, DeMello AJ. Microfluidic-assisted fiber production: potentials, limitations, and prospects. Biomicrofluidics. 2022;16(6):061504. [CrossRef].
104. Song Y, Yu XQ, Chen S. Recent advances in microfluidic fiber-spinning chemistry. J Polym Sci. 2024;62(3):447–62. [CrossRef].
105. Gonçalves RC, Oliveira MB, Mano JF. Exploring the potential of all-aqueous immiscible systems for preparing complex biomaterials and cellular constructs. Mater Horiz. 2024;11(19):4573–99. [CrossRef].
106. Yang C, Yu Y, Wang X, Shang L, Zhao Y. Programmable knot microfibers from piezoelectric microfluidics. Small. 2022;18(5):2104309. [CrossRef].
107. Ma W, Liu D, Ling S, Zhang J, Chen Z, Lu Y, et al. High-throughput and controllable fabrication of helical microfibers by hydrodynamically focusing flow. ACS Appl Mater Interfaces. 2021;13(49):59392–9. [CrossRef].
108. Yang C, Li W, Zhao Y, Shang L. Flexible liquid-diode microtubes from multimodal microfluidics. Proc Natl Acad Sci U S A. 2024;121(28):e2402331121. [CrossRef].
109. Wang H, Zhao Z, Liu Y, Shao C, Bian F, Zhao Y. Biomimetic enzyme cascade reaction system in microfluidic electrospray microcapsules. Sci Adv. 2018;4(6):eaat2816. [CrossRef].
110. de Rutte J, Dimatteo R, Archang MM, van Zee M, Koo D, Lee S, et al. Suspendable hydrogel nanovials for massively parallel single-cell functional analysis and sorting. ACS Nano. 2022;16(5):7242–57. [CrossRef].
111. Ghosh R, Arnheim A, van Zee M, Shang L, Soemardy C, Tang RC, et al. Lab on a particle technologies. Anal Chem. 2024;96(20):7817–39. [CrossRef].
112. Udani S, Langerman J, Koo D, Baghdasarian S, Cheng B, Kang S, et al. Associating growth factor secretions and transcriptomes of single cells in nanovials using SEC-seq. Nat Nanotechnol. 2024;19(3):354–63. [CrossRef].
113. Cai L, Chen G, Wang Y, Zhao C, Shang L, Zhao Y. Boston ivy-inspired disc-like adhesive microparticles for drug delivery. Research. 2021;2021:9895674. [CrossRef].
114. Nie M, Nagata S, Oda H, Takeuchi S. Millimeter-thick 3D tissues constructed by densely cellularized core-shell microfluidic bioprinting. Biofabrication. 2023;15(3):035010. [CrossRef].
115. Wang Y, Li J, Sun L, Chen H, Ye F, Zhao Y, et al. Liquid metal droplets-based elastomers from electric toothbrush-inspired revolving microfluidics. Adv Mater. 2023;35(20):e2211731. [CrossRef].

116. Zhang C, Duan Y, Jiao Z, Zhu Y, Xu B, Yang H, et al. Functional fluid-based soft robotic actuation. Adv Mater. 2025;37(34):2502669. [CrossRef].
117. Wang C, Zhao T, Cheng W, Ni Z, Xiang N. Microfluidic strategies in soft robotics: actuators, control systems, and pumps. Device. 2024;2(9):100551. [CrossRef].
118. Ding Z, Cai Y, Sun H, Rong X, Ye S, Fan J, et al. Janus hydrogel microrobots with bioactive ions for the regeneration of tendon-bone interface. Nat Commun. 2025;16(1):2189. [CrossRef].
119. Sun D, Guo B, Zhang A, Yang Z, Li H, Zhang J, et al. Microfluidic wet-spun core–shell elastomer fibers with integrated sensing and actuation capabilities. Small. 2025;21(48):e09817. [CrossRef].
120. Haney B, Werner JG, Weitz DA, Ramakrishnan S. Absorbent-adsorbates: large amphiphilic Janus microgels as droplet stabilizers. ACS Appl Mater Interfaces. 2020;12(29):33439–46. [CrossRef].
121. Dong Y, Wang L, Wang J, Wang S, Wang Y, Jin D, et al. Graphene-based helical micromotors constructed by "microscale liquid rope-coil effect" with microfluidics. ACS Nano. 2020;14(12):16600–13. [CrossRef].
122. Dong Y, Wang L, Zhang Z, Ji F, Chan TKF, Yang H, et al. Endoscope-assisted magnetic helical micromachine delivery for biofilm eradication in tympanostomy tube. Sci Adv. 2022;8(40):eabq8573. [CrossRef].